

Solving QCD Hamiltonian for bound states ¹

Elena Gubankova

*Institute of Theoretical and Experimental Physics, B. Cheremushkinskaya 25,
RU-117 218 Moscow, Russia*

Abstract

We consider the eigenstate problem for a Hamiltonian operator of the field theory. Methods of construction the effective field theoretical Hamiltonians for which the eigenstate problem may be solved are discussed. In particular, we discuss the method of flow equations from a general perspective as well as in application to the gauge field theories. Flow equations transform the Hamiltonian to a block-diagonal form with the number of particles conserved in each block and thus reduce the original bound state problem to a set of coupled eigenstate equations with an effective Hamiltonian in each sector.

Applications of flow equations to the Hamiltonians of QED and QCD in the light-front gauge and the QCD Hamiltonian in the Coulomb gauge are considered. Using flow equations, we derive the effective Hamiltonians as well as the renormalized gap equations and the Bethe-Salpeter equations for the bound states in these theories. We show that the obtained equations are finite in both UV and IR regions and are completely renormalized in UV, i.e. the corresponding solutions do not depend on the cut-off Λ .

We calculate positronium spectrum, glueball masses, $\pi - \rho$ mass splitting, gluon and chiral quark condensates and compare our results with the covariant calculations and experimental results. Use of flow equations to calculate the dynamical terms is critical to achieve good agreement with experimental results.

¹Based on talks given at JLAB (August 30, 1999), Duke University (October, 1999), BNL (November 3, 2000), MIT (December 11, 2001).

Contents

1	Flow equations. Idea and technique.	3
1.1	Hamiltonian bound state problem	3
1.2	Hamiltonian methods	3
1.2.1	Tamm-Dancoff truncation and iterated resolvents	4
1.2.2	Similarity renormalization	4
1.3	Flow equations	5
2	Application of flow equations to the gauge field theories	11
2.1	Flow equations in the light-front QED and QCD	11
2.1.1	Effective Hamiltonian for the light-front QED	13
2.1.2	Effective Hamiltonian for the light-front QCD	19
2.2	Flow equations for QCD in the Coulomb gauge	21
2.2.1	Flow equation scaling	21
2.2.2	Model calculations in QCD	22
2.2.3	Duality and BV transformation	23
2.2.4	QCD motivated Hamiltonian in the Coulomb gauge	23
2.2.5	Effective Hamiltonian for gluodynamics in the Coulomb gauge	24
2.2.6	Effective Hamiltonian for QCD in the Coulomb gauge	33
3	Conclusions	48

1 Flow equations. Idea and technique.

1.1 Hamiltonian bound state problem

Motivation

Nonabelian gauge field theories, like Quantum Chromodynamics (QCD), are well understood in the high-momentum region, since due to the asymptotic freedom coupling constant is small and Feynmann rules of the covariant perturbation theory, using L_{QCD} , provide convincing agreement with experiment. However, low energy QCD, where such nonperturbative phenomena as confinement and chiral symmetry breaking are taking place, is still understood only on a phenomenological level. Except for the lattice studies and some phenomenological models, there is a lack of analytical nonperturbative methods. Here a systematic analytical method to solve bound state problem, using Hamiltonian,

$$H_{QCD}|\psi\rangle = E|\psi\rangle, \quad (1)$$

is presented.

Problems

Two general problems occur when solving the eigenstate equation for a relativistic Hamiltonian of the field theory: field theoretical Hamiltonian is an infinite dimensional matrix, first, in the particle number space and, second, in the energy space.

First, the number of particles is not fixed in the field theory due to allowed creation and annihilation processes in vacuum. Therefore, any physical state contains, in principle, infinite many Fock components

$$|\psi\rangle_{meson} = c_{q\bar{q}}|q\bar{q}\rangle + c_{q\bar{q}g}|q\bar{q}g\rangle + \dots \quad (2)$$

Thus, we need a method to construct an effective Hamiltonian, which acts in a smaller truncated space and provides the same eigenvalues as the original Hamiltonian.

Second, there are states with (infinite) large energies/momenta in the Hamiltonian, which contribute UV divergent matrix elements. Hamiltonian matrix in a momentum space (plane wave space) reads

$$H = \begin{array}{c|c} 0 & \\ \hline & \Lambda \rightarrow \infty \end{array}, \quad (3)$$

where the top left matrix element correspond to small (zero) momentum, and the bottom right – to (infinite) large momentum with the cut-off UV scale Λ_{UV} . Thus, we need a method of UV regularization and subsequent renormalization directly for a Hamiltonian operator.

1.2 Hamiltonian methods

There are following Hamiltonian methods, which address both problems. However, there are some disadvantageous in these methods, restricting the range of their applicability.

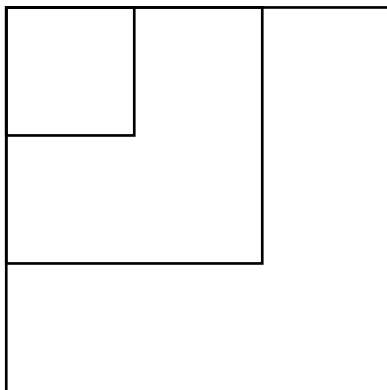


Figure 1: Projection of high Fock components to the low ones.

1.2.1 Tamm-Dancoff truncation and iterated resolvents

The method of Tamm-Dancoff truncation, treating the 'infinities' in Fock space, has been invented in 50's, and later generalized in the method of iterated resolvents by Pauli in 80's. The main idea of this method is to project high Fock components onto the lower ones in sequence, ending up with an effective Hamiltonian which acts in a smaller truncated space (Fig. 1) and therefore it can be solved for eigenstates and eigenvalues.

Technically, by projecting high Fock states one inverts a resolvent, which is the energy denominator containing matrix element of the original Hamiltonian, $(E - \langle n|H|m\rangle)^{-1}$. Inversion is done within some approximation scheme. It turns out that this scheme breaks down for QCD, convergence cannot be achieved, and eigenvalues of an effective QCD Hamiltonian do not predict QCD mass spectrum correctly. Physically, starting with a canonical QCD Hamiltonian and working in terms of bare fields, one fails to find a representation for the QCD Hamiltonian with fixed number of particles, since QCD vacuum is unstable and due to a strong QCD interaction it creates and annihilates bare particles. In addition, unregulated UV divergences, coming from high energies, appear in the effective Hamiltonian. A way out to proceed with QCD is suggested by various phenomenological studies, where instead of bare (current) degrees of freedom one uses the renormalized (constituent) ones. In other words, one needs a scheme to regulate and renormalize Hamiltonians.

1.2.2 Similarity renormalization

Several years ago, in 1994, the similarity renormalization scheme, which treats 'infinities' in the energy space, has been suggested by Glazek and Wilson. Similarity scheme is an analog to the Wilson's renormalization through an effective action where high energy modes integrated out in a path integral, but formulated directly for a Hamiltonian matrix. The aim is to regulate and renormalize away UV divergencies. The main idea of the similarity renormalization is to find a unitary transformation, U , which brings a Hamiltonian matrix to a band-diagonal form (Fig. 2) with the width of the band, λ ,

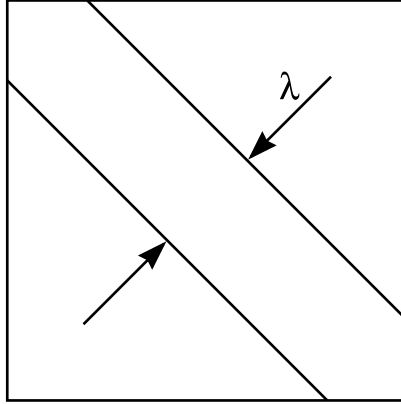


Figure 2: Band-diagonal Hamiltonian in the energy space.

being much smaller than the UV cut-off, Λ_{UV} ,

$$U^\dagger(\lambda, \Lambda)H(\Lambda)U(\lambda, \Lambda) = H_{eff}(\lambda, \Lambda) \quad (4)$$

$$|E_i - E_j|l\lambda \ll \Lambda .$$

High and low energy states decouple from each other in a band-diagonal effective Hamiltonian. Indeed, high order in the perturbation theory

$$g^{2\lambda/\Lambda} \ll 1, \quad (5)$$

with $\lambda \ll \Lambda$, connects high and low energies. Therefore, a low-energy effective Hamiltonian, H_{eff} , can be taken and solved for few lowest states. Since transformation is unitary, eigenvalues of H_{eff} should be the same as low lying states of the original Hamiltonian. Similarity renormalization is formulated as a perturbation expansion in coupling constant. As one shrinks the band width, λ , one breaks perturbation theory at some point, since diagonalization is a nonperturbative problem. In similarity, higher orders of perturbation theory correspond to higher Fock states. Therefore, breaking of the perturbation theory means that mixing of higher Fock components becomes important and cannot be neglected. In QED, a perturbative mixing of electron-positron and electron-positron-photon states provides reliable approximation for positronium bound states. Also, the window for the band width can be easily found, $m\alpha^2 \ll \lambda \ll m\alpha$ where $\alpha = e^2/4\pi$. However, for QCD a perturbative mixing does not work. One needs a nonperturbative scheme to incorporate high Fock states mixing.

1.3 Flow equations

Method of flow equations for Hamiltonians was suggested independently by Wegner in 1994. Applied to the field theory, flow equations try to solve both problems: 'infinities' in the Fock space as well as in the energy space. H_{eff} incorporates effects from high Fock components and large energies. This method can be viewed as a synthesis of the Tamm-Dancoff and similarity renormalization approaches. However, instead of

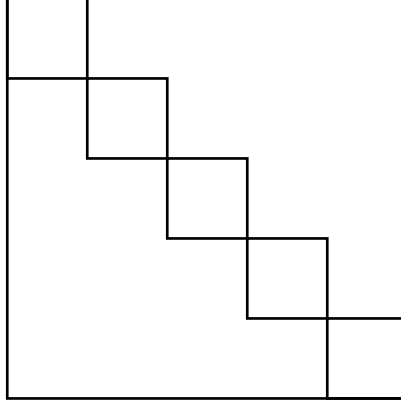


Figure 3: Block-diagonal Hamiltonian in the particle number space.

band-diagonalization in the energy space, that is hard to achieve, one block-diagonalizes Hamiltonian in the particle number space (Fig. 3).

One seeks for a unitary transformation, which brings a Hamiltonian matrix

$$H = \begin{pmatrix} PHP & PHQ \\ QHP & QHQ \end{pmatrix}, \quad (6)$$

where P and $Q = 1 - P$ are projection operators in the particle number space, to a block-diagonal form

$$H = \begin{pmatrix} PH_{eff}P & \\ & QH_{eff}Q \end{pmatrix}, \quad (7)$$

with the number of particles being conserved in each block. Since blocks decouple from each other in a block-diagonal effective Hamiltonian, full bound state problem is reduced to several eigenstate equations in each block. Usually it is easier to diagonalize separately P or Q sectors than to diagonalize the original Hamiltonian matrix.

Unitary transformation is governed by a continuous flow parameter l ,

$$U(l)HU^{-1}(l) = H(l), \quad (8)$$

with initial condition $U(l = 0) = 1$. As $l \rightarrow \infty$ an effective Hamiltonian coincides with its diagonal part, Eq. (7), $H(l \rightarrow \infty) = PH_{eff}P$. Unitary transformation is given by

$$U(l) = T_l \exp \left(\int_0^l \eta(l') dl' \right), \quad (9)$$

where $\eta(l)$ is the generator of transformation, and T_l is the l -ordering. Wegner's flow equations are written in a differential form

$$\begin{aligned} \frac{dH(l)}{dl} &= [\eta(l), H(l)] \\ \eta(l) &= [H_d(l), H(l)], \end{aligned} \quad (10)$$

where the generator, chosen by Wegner as a commutator of a diagonal part,

$$H_d(l) = \begin{pmatrix} PH(l)P & \\ & QH(l)Q \end{pmatrix}, \quad (11)$$

and an off-diagonal part,

$$H(l) - H_d(l) = \begin{pmatrix} & PH(l)Q \\ QH(l)P & \end{pmatrix}, \quad (12)$$

insures that an effective Hamiltonian is diagonal at $l \rightarrow \infty$, $H(l \rightarrow \infty) = H_d(l \rightarrow \infty)$. Diagonal – particle number conserving, Eq. (11), and off-diagonal – particle number changing, Eq. (12), parts of a Hamiltonian contain sector Hamiltonians which are functions of the flow parameter l .

Using Eqs. (10) and (11), (12), flow equations for the diagonal and off-diagonal Hamiltonians, and the generator of transformation are written in the operator form as

$$\begin{aligned} \frac{d}{dl} PHP &= P\eta QHP - PHQ\eta P \\ \frac{d}{dl} PHQ &= P\eta QHQ - PHP\eta Q \\ P\eta Q &= PHPHQ - PHQHQ. \end{aligned} \quad (13)$$

Choosing eigenstates of initial P and Q sector Hamiltonians for a basis (suppose it can be done), Eq. (13) is given in the matrix form

$$\begin{aligned} \frac{d}{dl} h_{pp'}(l) &= \sum_q (\eta_{pq}(l) h_{qp'}(l) - h_{pq}(l) \eta_{qp'}(l)) \\ \frac{d}{dl} h_{pq}(l) &= -(E_p(l) - E_q(l)) \eta_{pq}(l) \\ \eta_{pq}(l) &= (E_p(l) - E_q(l)) h_{pq}(l), \end{aligned} \quad (14)$$

with $PH(l)P \rightarrow E_p(l)$, $QH(l)Q \rightarrow E_q(l)$, and $PH(l)Q \rightarrow h_{pq}(l)$; p, p' are energy/momentum indices in the P space. Substituting the generator of transformation, we get a coupled system of equations for particle number conserving

$$\begin{aligned} \frac{dh_{pp'}(l)}{dl} &= -\sum_q \left(\frac{dh_{pq}(l)}{dl} \frac{h_{qp'}(l)}{E_p(l) - E_q(l)} + \frac{h_{pq}(l)}{E_{p'}(l) - E_q(l)} \frac{dh_{qp'}(l)}{dl} \right) \\ \frac{dE_p(l)}{dl} &= -\sum_q \frac{1}{E_p(l) - E_q(l)} \frac{d}{dl} (h_{pq}(l) h_{qp}(l)), \end{aligned} \quad (15)$$

and particle number changing sectors

$$\frac{dh_{pq}(l)}{dl} = -(E_p(l) - E_q(l))^2 h_{pq}(l), \quad (16)$$

respectively. Formal solution of these equations in P space is given at the flow parameter $l \rightarrow \infty$. Particle number conserving part

$$\begin{aligned} h_{pp'}(\infty) &= h_{pp'}(0) - \int_0^\infty dl \sum_q \left(\frac{dh_{pq}(l)}{dl} \frac{h_{qp'}(l)}{E_p(l) - E_q(l)} + \frac{h_{pq}(l)}{E_{p'}(l) - E_q(l)} \frac{dh_{qp'}(l)}{dl} \right) \\ E_p(l) &= E_p(0) - \int_0^l dl' \sum_q \frac{1}{E_p(l') - E_q(l')} \frac{d}{dl'} (h_{pq}(l') h_{qp}(l')) , \end{aligned} \quad (17)$$

includes the initial P sector Hamiltonian plus terms, generated by flow equations when eliminating particle number changing sector. If p corresponds to one-particle degree of freedom, the second equation in (17) is the energy gap equation, and the first equation is the Bethe-Salpeter integral equation for a bound state. Eq. (17) resembles the second order perturbation theory, where $h_{pq}(l)$ is a vertex and $1/(E_p(l) - E_q(l))$ is the energy denominator. It is important, that energies also flow with l , and are given by diagonal matrix elements in P space, $p = p'$. To find P space effective Hamiltonian, $h_{pp'}$, one should know l dependent solutions for the energies, $E_p(l)$ and $E_q(l)$, and for the particle number changing part, $h_{pq}(l)$. Solution for the particle number changing part

$$h_{pq}(l) = h_{pq}(0) \exp \left(- \int_0^l dl' (E_p(l') - E_q(l'))^2 \right) , \quad (18)$$

characterizes by an exponential function. For l -independent energies, h_{pq} decays exponentially to zero with $l \rightarrow \infty$. Renormalization of energies, i.e. l -dependence of energies, brings some additional factor before the exponential decay. Energy renormalization is crucial for degenerate matrix elements, when initially $|E_p(0) - E_q(0)| = 0$ for $l = 0$. In this case, l -dependence of energies provides power law decay of h_{pq} instead of exponential one. Thus, the Wegner's generator (Eq. (10)) insures that the off-diagonal part is eliminated always, even for degenerate states. Eqs. (17) and (18) are coupled, therefore they should be solved selfconsistently.

Our strategy is to solve first the equation for an effective renormalized energy (the gap equation), and then using energy solutions to find an effective Hamiltonian in P -sector, $h_{pp'}$, (kernel of the Bethe-Salpeter equation), which is diagonalized numerically for bound states. Success of the procedure depends on a particular choice of diagonal and off-diagonal Hamiltonian parts, that is discussed in application to QED and QCD further.

In a block-diagonal Hamiltonian, there is some freedom left to transform inside of each block without changing a block-diagonal structure. This freedom can be used by choosing different similarity functions, $f(x)$,

$$\begin{aligned} h_{pq}(l) &= h_{pq}(0) f(x_{pq}) \\ x_{pq}(l) &= \int_0^l dl' (E_p(l') - E_q(l'))^2 , \end{aligned} \quad (19)$$

with general properties to be equal unity at the origin, and to fall down at large arguments

$$f(0) = 1 , f(x \rightarrow \infty) = 0 . \quad (20)$$

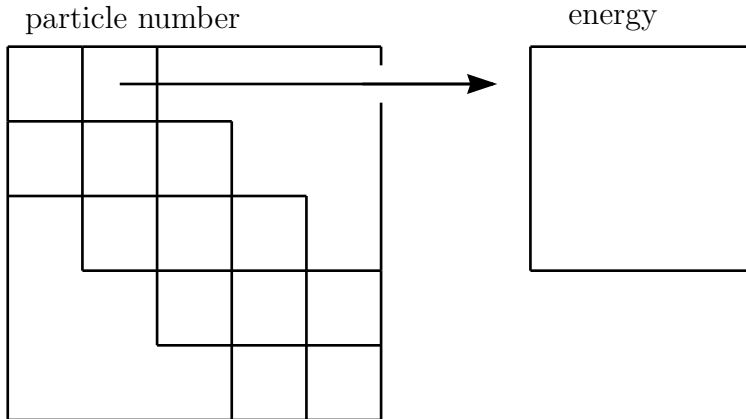


Figure 4: Pentadiagonal form of Hamiltonian in the particle number space; each sector contains matrix elements with all possible energy changes.

Similarity function reflects the rate how quickly the particle number changing sector is eliminated. The generator is written through the similarity function as

$$\eta_{pq}(l) = -\frac{h_{pq}(l)}{E_p(l) - E_q(l)} \frac{d}{dl} (\ln f_{pq}(x)) , \quad (21)$$

$f_{pq}(x) = f(x_{pq})$. Flow equation scheme with P and Q sectors can be easily generalized to the case of many Fock components (Fig. 4). It is important, that the relevant degrees of freedom are renormalized during this procedure. As a consequence, it is not coupling constant which is used as a small parameter, but rather some dimensionless combination, say $x_{pq} = |h_{pq}|/|E_p - E_q|$.

Elimination of the particle number changing sectors is carried out not in one step but sequentially for energy differences which exceed the band width λ (flowing cut-off), Eq. (18),

$$\lambda = \frac{1}{\sqrt{l}} \leq |E_p(0) - E_q(0)| \leq \frac{1}{\sqrt{l \rightarrow 0}} = \Lambda \rightarrow \infty , \quad (22)$$

for l -independent energies, with $l = 1/\lambda^2$ (Fig. 5).

Lowering the cut-off λ , we effectively scale the theory down to low energies, that provides a connection between flow equations and similarity renormalization. System of coupled flow equations contain equations of the renormalization group, in addition to appearing equations for noncanonical operators. In this way, we incorporate renormalization in the many-body technique of block-diagonalizing.

Summary I

1) Summarizing, flow equations perform Hamiltonian 'renormalization' in the energy and particle number space, in the sense that an effective Hamiltonian is finite in both spaces and contains effects of high energies and high Fock components. Technically, flow equations allow to include directly the dynamical perturbative corrections, responsible for the renormalization and the UV asymptotic region, into the many-body calculations.

2) For the first time, due to the dynamical interactions, the physical equations are obtained UV and IR finite.

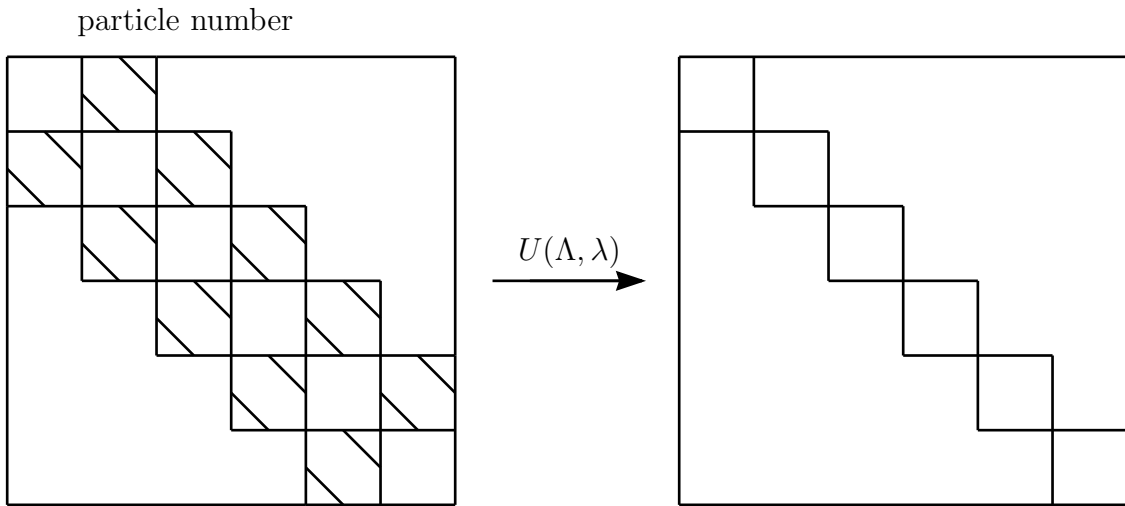


Figure 5: Flow equations block-diagonalize the bare regulated by Λ Hamiltonian ($H(\Lambda)$) in the particle number space. For the finite λ (after the unitary transformation $U(\Lambda \rightarrow \infty, \lambda)$ is performed) the matrix elements of the particle number changing sectors are squeezed in the energy band $|E_i - E_j| < \lambda$ on the left hand side the picture and are eliminated completely as $\lambda \rightarrow 0$ (that corresponds to $U(\Lambda \rightarrow \infty, \lambda \rightarrow 0)$) on the right hand side of the picture. Block-diagonal effective Hamiltonian is also UV renormalized by flow equations.

2 Application of flow equations to the gauge field theories

Flow equations have been applied mostly in solid state physics by Wegner and his group. Also some toy models have been considered in the field theory. Here we consider several examples in the gauge field theories, such as the light-front QED [1] and light-front QCD [2] Hamiltonians as well as Hamiltonian of gluodynamics [3] and QCD Hamiltonian with dynamical quarks [4] in the Coulomb gauge. In Hamiltonian dynamics of the gauge field theory, first a gauge should be fixed and constraint equations should be solved. Hamiltonian operator is expressed only through the physical degrees of freedom. Generally fewer equations of motion and current algebra relations (like Ward identities) occur in the Hamiltonian dynamics than for an effective action. Moreover, there are no ambiguities in these equations since the physical fields have been used. However, one should keep track on covariance and gauge invariance manifest for physical observables. This serves to check the validity of the calculations and approximations.

2.1 Flow equations in the light-front QED and QCD

Light-front dynamics is similar to the equal time one, except that the light-front time is given by $x^+ = t + z$, and the commutation relations and initial conditions are formulated at a quantization plane $x^+ = 0$, instead of $t = 0$ in the equal time framework. Evolution (propagation) is considered along the light-front, $0 < x^+$. In the collinear limit (small light-front x) which corresponds to the light-front origin point, the light-front field theory has a singular behavior associated with nontrivial vacuum effects in the equal time.

The Lagrangian density for QED/QCD

$$\mathcal{L} = -\frac{1}{4}F_{\mu\nu}F^{\mu\nu} + \bar{\psi}(i \not{\partial} + g \not{A} - m)\psi \quad (23)$$

is considered here in the light-cone gauge $A^+ = A^0 + A^3 = 0$. Zero modes will be disregarded. The constrained degrees of freedom, A^- and ψ_- ($\Lambda_{\pm} = \frac{1}{2}\gamma^0\gamma^{\pm}$ are projection operators, thus $\psi_{\pm} = \Lambda_{\pm}\psi$, and $\psi = \psi_+ + \psi_-$) are removed explicitly and produce the canonical QED/QCD Hamiltonian. It is defined through the independent physical fields A_{\perp} and ψ_+ . To solve the constrained equations for A^- and ψ_- the auxiliary fields

$$\begin{aligned} \tilde{A}_+ &= A_+ - \frac{g}{(i\partial^+)^2} J^+, \\ \tilde{\Psi} &= \Psi_+ + (m\beta - i\alpha^i\partial_{\perp i}) \frac{1}{2i\partial_-} \Psi_+, \end{aligned} \quad (24)$$

are introduced. The fermion current is $\tilde{J}^{\mu}(x) = \tilde{\bar{\Psi}}\gamma^{\mu}\tilde{\Psi}$. The resulting canonical Hamiltonian $H = P_+$ is given as a sum of the free Hamiltonian and the interaction

$$H = P_+ = H_0 + V + W. \quad (25)$$

The free Hamiltonian H_0 , the quark and gluon kinetic energies, is

$$H_0 = \frac{1}{2} \int dx_+ d^2x_{\perp} \left(\tilde{\bar{\Psi}}\gamma^+ \frac{m^2 + (i\nabla_{\perp})^2}{i\partial^+} \tilde{\Psi} + \tilde{A}^{\mu}(i\nabla_{\perp})^2 \tilde{A}_{\mu} \right). \quad (26)$$

In the interaction $V + W$, the vertex interaction V is the light-cone analogue of the minimal coupling interaction in covariant QED/QCD and $W = W_1 + W_2$ is the sum of the instantaneous-gluon W_1 and the instantaneous-quark interactions W_2 . The latter arise from the constraint equations (analog of the light-front Gauss law). More explicitly, the interaction is given by

$$\begin{aligned}
V &= g \int dx_+ d^2 x_\perp \tilde{J}^\mu \tilde{A}_\mu, \\
W_1 &= \frac{g^2}{2} \int dx_+ d^2 x_\perp \tilde{J}^+ \frac{1}{(i\partial^+)^2} \tilde{J}^+, \\
W_2 &= \frac{g^2}{2} \int dx_+ d^2 x_\perp \tilde{\Psi} \gamma^\mu \tilde{A}_\mu \frac{\gamma^+}{i\partial^+} (\gamma^\nu \tilde{A}_\nu \tilde{\Psi}), \\
V' &= \int dx_+ d^2 x_\perp \tilde{B}_a^{\mu\nu} \tilde{B}_{\mu\nu}^a,
\end{aligned} \tag{27}$$

where the current includes the quark and gluon parts

$$\tilde{J}^\mu(x) = \tilde{\Psi} \gamma^\mu \tilde{\Psi} T^a + \frac{1}{i} [\tilde{F}^{\mu k}, \tilde{A}_k], \tag{28}$$

with $\tilde{A}_\mu = A_\mu^a T^a$. The instantaneous gluon and quark interactions behave as $1/q^{+2}$ and $1/q^+$, respectively, with the momentum transfer $q = (q_+, q_\perp)$.

It is convenient to work in a second quantized form, decomposing the physical fields through creation and annihilation operators. By definition, the fields $\tilde{\Psi} = \tilde{\Psi}_+ + \tilde{\Psi}_-$ and $\tilde{A}^\mu = (0, \tilde{A}_\perp, \tilde{A}^+)$ are the free solutions which in momentum space are parametrized as

$$\begin{aligned}
\tilde{\Psi}_\alpha(x) &= \sum_\lambda \int \frac{dp^+ d^2 p_\perp}{\sqrt{2p^+(2\pi)^3}} \left(b(p) u_\alpha(p, \lambda) e^{-ipx} + d^\dagger(p) v_\alpha(p, \lambda) e^{+ipx} \right), \\
\tilde{A}_\mu(x) &= \sum_\lambda \int \frac{dp^+ d^2 p_\perp}{\sqrt{2p^+(2\pi)^3}} \left(a(p) \epsilon_\mu(p, \lambda) e^{-ipx} + a^\dagger(p) \epsilon_\mu^*(p, \lambda) e^{+ipx} \right).
\end{aligned} \tag{29}$$

The single particle operators obey the commutation relations

$$[a(p), a^\dagger(p')] = \{b(p), b^\dagger(p')\} = \{d(p), d^\dagger(p')\} = \delta(p^+ - p'^+) \delta^{(2)}(\vec{p}_\perp - \vec{p}'_\perp) \delta_\lambda^{\lambda'}. \tag{30}$$

The free part is given by

$$\widehat{H}_0(l) = \int \frac{[d^3 p]}{\sqrt{2p^+}} E(p; l) \left(b^\dagger(p) b(p) + d^\dagger(p) d(p) \right) + \int \frac{[d^3 p]}{\sqrt{2p^+}} \omega(p; l) a^\dagger(p) a(p). \tag{31}$$

The single particle energies ($E = p^-$) depend on the 3-momentum $p = (p^+, \vec{p}_\perp)$

$$E(p; l) = \frac{\vec{p}_\perp^2 + m^2(p; l)}{p^+}, \quad \omega(p; l) = \frac{\vec{p}_\perp^2 + \mu^2(p; l)}{p^+}, \tag{32}$$

and potentially on the flow parameter through the mass $m^2(p; l)$ of the particle in question. Inserting the free fields into the Hamiltonian yields for the quark-gluon vertex interaction

$$\begin{aligned}
\widehat{V}(l) &= \frac{1}{\sqrt{(2\pi)^3}} \int \frac{[d^3 p_1]}{\sqrt{2p_1^+}} \int \frac{[d^3 p_2]}{\sqrt{2p_2^+}} \int \frac{[d^3 p_3]}{\sqrt{2p_3^+}} \delta^{(3)}(p_1 - p_2 - p_3) \\
&\quad \left[g(p_1, p_2, p_3; l) b^\dagger(p_1) b(p_2) a(p_3) \bar{u}(p_1) \not{\epsilon}(p_3) u(p_2) + \dots \right],
\end{aligned} \tag{33}$$

and the quark-antiquark interaction in the exchange channel

$$\begin{aligned} \widehat{W}_{e\bar{e}}(l) &= \frac{1}{(2\pi)^3} \int \frac{[d^3 p_1]}{\sqrt{2p_1^+}} \int \frac{[d^3 p_2]}{\sqrt{2p_2^+}} \int \frac{[d^3 p_3]}{\sqrt{2p_3^+}} \int \frac{[d^3 p_4]}{\sqrt{2p_4^+}} \delta^{(3)}(p_1 - p_2 + p_3 - p_4) \\ &\quad \left[W_{\mu\nu}(p_1, p_2, p_3, p_4; l) b^\dagger(p_1) b(p_2) d(-p_3) d^\dagger(-p_4) T_{12}^a T_{34}^a \right. \\ &\quad \left. \bar{u}(p_1) \gamma^\mu u(p_2) \bar{v}(-p_3) \gamma^\nu v(-p_4) + \dots \right]. \end{aligned} \quad (34)$$

The integration symbols denote

$$[d^3 p] = dp^+ d^2 p_\perp \sum_\lambda, \quad (35)$$

and the abbreviations $u(p) \equiv u(p, \lambda)$ and $\not{\epsilon}^* \equiv \gamma^\mu \epsilon \mu^*(p, \lambda)$ are introduced. When unitary transformation with the finite flow parameter l is applied, all coupling constants and masses become unknown functions of momenta and l (This is reflected in explicit dependence of g and m , μ , and $W_{\mu\nu}$). Initial conditions are given at $l = 0$. The effective coupling constant has the initial value

$$g(l = 0) = g, \quad (36)$$

with the fine structure constant $\alpha = g^2/4\pi \sim 1/137$ in QED, and the strong coupling $g = g_s$ in QCD. The two-point interaction includes the instantaneous and dynamical generated by flow equations interactions, $W = W^{inst} + W^{gen}$, with initial conditions

$$W_{\mu\nu}^{inst}(l = 0) = -\frac{\eta_\mu \eta_\nu}{q^{+2}}, \quad W_{\mu\nu}^{gen}(l = 0) = 0, \quad (37)$$

where the momentum transfer is $q = p_1 - p_2$.

2.1.1 Effective Hamiltonian for the light-front QED

Representing through creation and annihilation operators, we define explicitly the particle number conserving and particle number changing parts which directly define the generator of transformation. In QED, all canonical interactions are shown in the Table 1; for example, the electron-photon minimal coupling is the matrix element H_{12} , the electron and photon instantaneous interactions are H_{14} and H_{22} , respectively. Particle number changing terms are off-diagonal in this table and are eliminated using flow equations.

The generator of the unitary transformation is

$$\widehat{\eta}(l) = \widehat{\eta}_1(l) + \widehat{\eta}_2(l). \quad (38)$$

where the generator $\widehat{\eta}_1 = [\widehat{H}_0, \widehat{V}]$ eliminates the electron-photon coupling V and is given by

$$\begin{aligned} \widehat{\eta}_1(l) &= \frac{1}{\sqrt{(2\pi)^3}} \int \frac{[d^3 p_1]}{\sqrt{2p_1^+}} \int \frac{[d^3 p_2]}{\sqrt{2p_2^+}} \int \frac{[d^3 p_3]}{\sqrt{2p_3^+}} \delta^{(3)}(p_1 - p_2 - p_3) \\ &\quad \times \left[\eta(p_1, p_2, p_3; l) b_1^\dagger b_2 a_3 \bar{u}(p_1) \not{\epsilon}(p_3) u(p_2) + \dots \right], \end{aligned} \quad (39)$$

	$ \gamma\rangle$	$ e\bar{e}\rangle$	$ \gamma\gamma\rangle$	$ e\bar{e}\gamma\rangle$	$ e\bar{e}e\bar{e}\rangle$
$ \gamma\rangle$					
$ e\bar{e}\rangle$					
$ \gamma\gamma\rangle$					
$ e\bar{e}\gamma\rangle$					
$ e\bar{e}e\bar{e}\rangle$					

Table 1: QED canonical Hamiltonian in the light-front gauge.


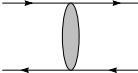
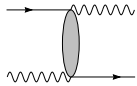
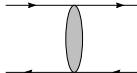
	$ \gamma\rangle$	$ e\bar{e}\rangle$	$ \gamma\gamma\rangle$	$ e\bar{e}\gamma\rangle$	$ e\bar{e}e\bar{e}\rangle$
$ \gamma\rangle$					
$ e\bar{e}\rangle$					
$ \gamma\gamma\rangle$					
$ e\bar{e}\gamma\rangle$					
$ e\bar{e}e\bar{e}\rangle$					

Table 2: Effective QED Hamiltonian generated through the second order by flow equations in the light-front gauge.

and the generator $\widehat{\eta}_2 = [\widehat{H}_0, \widehat{W}]$ eliminates the off-diagonal two-point interactions and its explicit form depends on the particular sector where is \widehat{W} .

QED coupling is a small parameter. Eliminating the particle number changing sector to the second order in coupling, we generate new terms which are given in the Table 2. In the second order $O(g^2)$, new dynamical two-point interactions arise from elimination the electron-photon vertex terms, while elimination of the instantaneous terms W generates new interactions in the third and high orders which are not depicted. In the Table 2, black area in the two-point interaction depicts an effective kernel which depends on all four in- and out-going momenta.

Effective electron-positron interaction (matrix element H_{22}) includes the instantaneous and dynamically generated by flow equations terms. In the exchange channel, it is given by a product of the current-current term and the interaction kernel,

$$W_{e\bar{e}} = -4\pi\alpha_s C_f \langle \gamma^\mu \gamma^\nu \rangle B_{\mu\nu}, \quad (40)$$

where the photon interaction kernel

$$B_{\mu\nu} = g_{\mu\nu} (I_1 + I_2) + \eta_\mu \eta_\nu \frac{\delta Q^2}{q^{+2}} (I_1 - I_2), \quad (41)$$

contains the integrals I_1 and I_2 which are defined by two similarity form factors in each vertex

$$I_1 = \int_0^\infty d\lambda \frac{1}{Q_1^2} \frac{df(Q_1^2; \lambda)}{d\lambda} f(Q_2^2; \lambda), \quad (42)$$

and for I_2 the indices 1 and 2 are interchanged. Here, Q_1^2 and Q_2^2 are momenta transfers in two vertexes. In the light-front framework, they are given by

$$\begin{aligned} Q_1^2 &= \frac{(x' k_\perp - x k'_\perp)^2 + m^2 (x - x')^2}{x x'} \\ Q_2^2 &= Q_1^2 |_{x \rightarrow (1-x); x' \rightarrow (1-x')}, \end{aligned} \quad (43)$$

On mass shell, these momenta are reduced to the three photon momentum transfer,

$$Q_1^2 = Q_2^2 \rightarrow \bar{q}^2. \quad (44)$$

Using three choices of similarity function; exponential $f = \exp(-Q^2/\lambda^2)$, gaussian $f = \exp(-Q^4/\lambda^4)$ and sharp $f = \theta(1 - Q^2/\lambda^2)$; we obtain the following kernels for the effective electron-positron interaction,

$$\begin{aligned} B_{\mu\nu} &= g_{\mu\nu} \frac{1}{Q^2} \\ B_{\mu\nu} &= g_{\mu\nu} \frac{1}{Q^2} - \left[\frac{g_{\mu\nu}}{Q^2} - \frac{\eta_\mu \eta_\nu}{q^{+2}} \right] \frac{\delta Q^4}{Q^4 + \delta Q^4} \\ B_{\mu\nu} &= g_{\mu\nu} \frac{1}{Q^2} - \left[\frac{g_{\mu\nu}}{Q^2} - \frac{\eta_\mu \eta_\nu}{q^{+2}} \right] \frac{|\delta Q^2|}{Q^2 + |\delta Q^2|}, \end{aligned} \quad (45)$$

respectively. Here, Q^2 is the average momentum transfer and δQ^2 shows the off-shellness. On the energy shell, i.e. $\delta Q^2 = 0$, the electron-positron interaction is reduced in each case to the 3-d Coloumb potential with behavior $1/\bar{q}^2$.

Picking the $e\bar{e}$ -sector, we solve an effective interaction for positronium bound states. The light front Schrödinger equation for the positronium model reads

$$H_{LC}|\psi_n \rangle = M_n^2|\psi_n \rangle, \quad (46)$$

where $H_{LC} = P^\mu P_\mu$ is the invariant mass (squared) operator, referred for convenience to as the light front Hamiltonian of positronium and $|\psi_n \rangle$ being the corresponding eigenfunction; n labels all the quantum numbers of the state. Projecting this equation on the $e\bar{e}$ state yields

$$H_{LC}^{eff}|(e\bar{e})_n \rangle = M_n^2|(e\bar{e})_n \rangle \dots \quad (47)$$

In the $e\bar{e}$ sector, the effective light-front Hamiltonian consists of the free part and the effective electron-positron interaction

$$H_{LC}^{eff} = H_{LC}^{(0)} + V_{LC}^{eff}, \quad (48)$$

The light front equation Eq. (47) is then expressed by the integral equation

$$\begin{aligned} & \left(\frac{m^2 + \vec{k}'^2}{x'(1-x')} - M_n^2 \right) \psi_n(x', \vec{k}'_\perp; s_3, s_4) \\ & + \sum_{s_1, s_2} \int_D \frac{dx d^2 k_\perp}{2(2\pi)^3} \langle x', \vec{k}'_\perp; s_3, s_4 | V_{LC}^{eff} | x, \vec{k}_\perp; s_1, s_2 \rangle \psi_n(x, \vec{k}_\perp; s_1, s_2) = 0, \end{aligned} \quad (49)$$

where the integration domain D is restricted by the covariant cutoff condition of Brodsky and Lepage

$$\frac{m^2 + \vec{k}^2}{x(1-x)} \leq \Lambda^2 + 4m^2, \quad (50)$$

allowing for states which have a kinetic energy below the cutoff Λ . The effective $e\bar{e}$ interaction, V_{LC}^{eff} , contains two-point dynamical and instantaneous interactions (with the kernel $W_{e\bar{e}}$ given by Eqs. (40) and (45)) as well as the electron self-energy terms in $e\bar{e}$ sector which are renormalized by the electron mass counterterm. We include the exchange and annihilation channels in the effective interaction, $V_{LC}^{eff} = V_{exch} + V_{ann}$.

Numerical solution of the integral equation (49) produces positronium spectrum, without (Fig. 6) and with (Fig. 7) annihilation channel. Including the annihilation channel, we obtain for the singlet-triplet splitting a surprising agreement with the equal time calculations. Degeneracy of triplet state shows that though calculations are done in the light-front framework the rotational invariance is manifest. Next excited states ($n = 2$) also show good agreement with the results of the equal time perturbation theory.

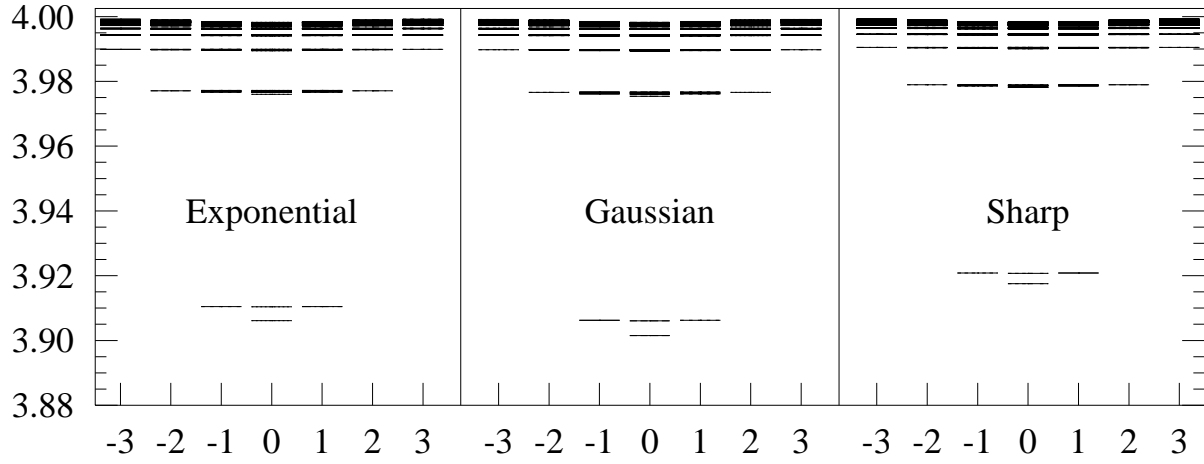


Figure 6: The invariant mass-squared spectrum M_i^2 for positronium versus the projection of the total spin, J_z , excluding annihilation with exponential, Gaussian and sharp cutoffs. The number of integration points is $N_1 = N_2 = 21$.

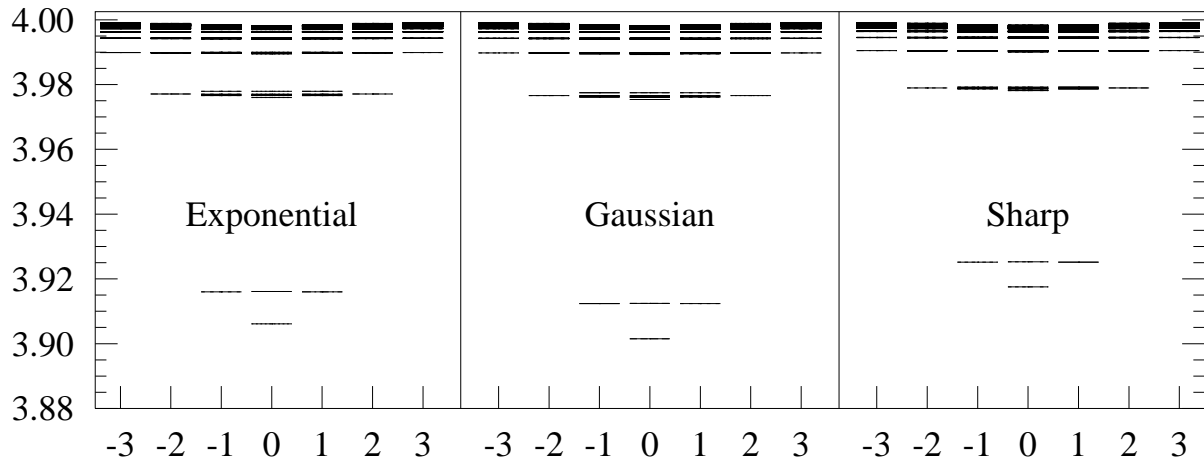


Figure 7: The invariant mass-squared spectrum M_i^2 for positronium versus the projection of the total spin, J_z , including annihilation with exponential, Gaussian and sharp cutoffs. The number of integration points is $N_1 = N_2 = 21$.

2.1.2 Effective Hamiltonian for the light-front QCD

QED calculations have been done in terms of bare unrenormalized parameters and success of these calculations is based on applicability of perturbation theory in terms of small QED charge. The same naive picture does not hold for QCD; coupling constant is strong. However, as we show below (see [2] for details), renormalization of the gluon energies might change the situation and QCD calculations can be still made using flow equations.

The effective quark-antiquark interaction including instantaneous and dynamically generated by flow equations terms is given by

$$V_{q\bar{q}} = -4\pi\alpha_s C_f \langle \gamma^\mu \gamma^\nu \rangle B_{\mu\nu}, \quad (51)$$

which formally coincides with the equation (40) for the $e\bar{e}$ interaction in QED. However, the gluon interaction kernel is given by

$$B_{\mu\nu} = \lim_{\mu_0, \lambda_0 \rightarrow 0} \left[g_{\mu\nu} (I_1 + I_2) + \eta_\mu \eta_\nu \frac{\delta Q^2}{q^2} (I_1 - I_2) \right], \quad (52)$$

where the integrals I_1 and I_2 are defined by two similarity form factors containing the cut-off dependent momenta transfer in each vertex,

$$I_1 = \int_0^\infty d\lambda \frac{1}{Q_1^2(\lambda)} \frac{df(Q_1^2(\lambda); \lambda)}{d\lambda} f(Q_2^2(\lambda); \lambda), \quad (53)$$

and with interchange 1 and 2 indices for I_2 . The gluon interaction kernel Eq. (52)) is defined in the limit of zero gluon mass, $\mu_0 = 0$, and zero renormalization point, $\lambda_0 = 0$, that is the renormalization condition in the gluon gap equation (see below). In the light-front framework, momenta transfer are given by

$$\begin{aligned} Q_1^2(\lambda) &= \frac{(x'k_\perp - xk'_\perp)^2 + m^2(x - x')^2}{xx'} + \mu_{ren}^2(\lambda) \\ Q_2^2(\lambda) &= Q_1^2(\lambda)|_{x \rightarrow (1-x); x' \rightarrow (1-x')}, \end{aligned} \quad (54)$$

where $\mu_{ren}(\lambda)$ is the renormalized gluon mass. On mass shell, momenta transfer are reduced to an effective gluon energy,

$$Q_1^2(\lambda) = Q_2^2(\lambda) \rightarrow \vec{q}^2 + \mu_{ren}^2(\lambda), \quad (55)$$

which contains three gluon momentum transfer and the renormalized gluon mass. Due to the presence of the renormalized gluon mass flow equations eliminate off-diagonal matrix elements even for vanishing gluon momenta, $\vec{q} = 0$, that corresponds to degenerate states. This cannot be achieved within perturbation theory (PT), since it breaks down at $\vec{q} = 0$ and an effective interaction has zero energy denominators. Nontrivial solution for the effective gluon mass (gluon gap) is a consequence of a special behavior of the light-front QCD in the collinear limit, $x^+ \rightarrow 0$, in the contrary to QED (there is no mass gap in QED). As mentioned before, this behavior of QCD might be attributed to QCD vacuum effects.

The renormalized gluon mass is defined as a solution of the gluon gap equation, $\mu(\lambda)$, renormalized by the canonical gluon mass counterterm of the perturbation theory, m_{CT} ,

$$\mu_{ren}^2(\lambda) = \mu^2(\lambda) + m_{CT}^2(\lambda). \quad (56)$$

One-point flow equations for the light-front energies provide the gap equations for the quark (m^2) and gluon (μ^2) renormalized masses

$$\begin{aligned}
\frac{dm^2(\lambda)}{d\lambda} &= C_f \int_0^1 \frac{dx}{x(1-x)} \int_0^\infty \frac{d^2 k_\perp}{16\pi^3} g_q^2(\lambda) \frac{1}{Q_3^2(\lambda)} \frac{df^2(Q_3^2(\lambda); \lambda)}{d\lambda} \\
&\times \left[k_\perp^2 \left(\frac{2}{1-x} + \frac{4}{x^2} \right) + 2m^2(\lambda) \frac{x^2}{1-x} \right] \\
\frac{d\mu^2(\lambda)}{d\lambda} &= 2T_f N_f \int_0^1 \frac{dx}{x(1-x)} \int_0^\infty \frac{d^2 k_\perp}{16\pi^3} g_q^2(\lambda) \frac{1}{Q_2^2(\lambda)} \frac{df^2(Q_2^2(\lambda); \lambda)}{d\lambda} \\
&\times \left[\frac{k_\perp^2 + m^2}{x(1-x)} - 2k_\perp^2 \right] \\
&+ 2C_a \int_0^1 \frac{dx}{x(1-x)} \int_0^\infty \frac{d^2 k_\perp}{16\pi^3} g_g^2(\lambda) \frac{1}{Q_1^2(\lambda)} \frac{df^2(Q_1^2(\lambda); \lambda)}{d\lambda} \\
&\times \left[k_\perp^2 \left(1 + \frac{1}{x^2} + \frac{1}{(1-x)^2} \right) \right], \tag{57}
\end{aligned}$$

where energies are given by

$$\begin{aligned}
Q_1^2(\lambda) &= \frac{k_\perp^2 + \mu^2(\lambda)}{x(1-x)} - \mu^2(\lambda) \\
Q_2^2(\lambda) &= \frac{k_\perp^2 + m^2}{x(1-x)} - \mu^2(\lambda) \\
Q_3^2(\lambda) &= \frac{k_\perp^2 + m^2(\lambda)}{x} + \frac{k_\perp^2 + \mu^2(\lambda)}{(1-x)} - m^2(\lambda). \tag{58}
\end{aligned}$$

These equations (57) are coupled, since unknown cut-off dependent quark and gluon masses enter the r.h.s. of both equations. The energy denominators, Eq. (58), show a one-loop structure. When expanded in the coupling constant at large cut-offs, $\lambda = \Lambda_{UV}$, these equations are reduced to the Dyson-Schwinger equation in the rainbow approximation. We solve the gluon gap equation with a constant current quark mass, using special prescription to regulate collinear small light-front x in the integral over dx . Absorbing trivial perturbative cut-off behavior by a canonical mass counterterm, Eq. (56), we obtain the renormalized cut-off dependent effective gluon mass.

Taking into account the cut-off dependent renormalized gluon mass, the quark-antiquark interaction (Eq. (52)) has the following form with three choices of similarity function,

$$\begin{aligned}
B_{\mu\nu} &= g_{\mu\nu} \left[\frac{1}{Q^2} + \frac{\sigma}{Q^4} \right] + \left[\frac{g_{\mu\nu}}{Q^2} - \frac{\eta_\mu \eta_\nu}{q^{+2}} \right] \frac{\sigma}{Q^2} \frac{\delta Q^4}{Q^4 - \delta Q^4} \\
B_{\mu\nu} &= g_{\mu\nu} \left[\frac{1}{Q^2} + \frac{\sigma}{Q^4} \right] - \left[\frac{g_{\mu\nu}}{Q^2} \left(1 + \frac{\sigma}{Q^2} \right) - \frac{\eta_\mu \eta_\nu}{q^{+2}} \right] \frac{\delta Q^4}{Q^4 + \delta Q^4} \\
B_{\mu\nu} &= g_{\mu\nu} \left[\frac{1}{Q^2} + \frac{\sigma}{Q^4} \right] - \left[\frac{g_{\mu\nu}}{Q^2} \left(1 + \frac{\sigma}{Q^2} \left(1 + \frac{Q^2}{Q^2 + |\delta Q^2|} \right) \right) \right. \\
&\quad \left. - \frac{\eta_\mu \eta_\nu}{q^{+2}} \left(1 + \frac{\sigma}{Q^2} \frac{Q^2}{Q^2 + |\delta Q^2|} \right) \right] \frac{|\delta Q^2|}{Q^2 + |\delta Q^2|}, \tag{59}
\end{aligned}$$

that should be compared with the electron-positron interaction in QED, Eq. (45). On the energy shell, the $q\bar{q}$ interaction is reduced to the sum of the Coulomb, $1/\vec{q}^2$, and linear confining, $1/\vec{q}^4$, potentials. Here, σ plays the role of the string tension depending on the cut-off which regulates small light-front x . This result cannot be obtained in the perturbation theory by naive summation over perturbative gluon exchanges in a few low orders. There are complex calculations, where infinite orders of given subclasses of diagrams result in a confining interaction.

Summary II

1) Though calculations are performed in the fixed light-front gauge where the light-front and perpendicular coordinates are treated differently, we obtain the covariant result using flow equations (triplet states are degenerate; effective interaction depends on the covariant four-momenta Q^2 and δQ^2). Dynamical terms generated by flow equations are crucial to maintain covariance.

2) Flow equations allow to obtain results beyond the perturbation theory. Also, a covariant result corresponding to resummation of large number of perturbative diagrams may be obtained by flow equations straightforward.

3) Flow equations allow to track the covariance and gauge invariance much easier than in the standard perturbation theory. (To maintain covariance in the PT, all diagrams in the given order including crossed diagrams should be summed. Except for the planar diagrams summation of high orders of PT is a problem.)

2.2 Flow equations for QCD in the Coulomb gauge

2.2.1 Flow equation scaling

Flow equations eliminate matrix elements which couple states with large energy differences, greater than $1/\sqrt{l} = \lambda$, and later more degenerate states. This is reminiscent of the energy scaling separation underlying perturbative scaling. Flow equations treats different energies separately, starting from UV and scaling down towards low energies, separating physics at each characteristic scale.

In strong interactions/QCD, moving from UV to IR, we encounter the following characteristic scales and corresponding regimes: at Λ_{UV} the conformal canonical perturbation theory (PT) without any scale and with bare quarks and gluons as degrees of freedom; at Λ_{QCD} PT breaks down due to the dimensional transmutation in the renormalization group (RG) (Λ_{QCD} is the RG invariant scale); at $\sqrt{\sigma}$ confinement sets in and hadron bound states (instead of quarks and gluons) become relevant degrees of freedom; at m_π chiral symmetry dynamically breaks, leading to the Goldstone boson-pion; nuclear physics decouples further down the scale with N and π as degrees of freedom. Physical ranges decouple from each other due to weak interaction (say in the chiral PT, interaction between the Goldstone mode and hadrons is weak). Flow equations decouple these regions, providing dynamics on all energy scales including crossover between weak and strong coupling.

In what follows, we consider regime where physics is dictated by phenomena of confinement and chiral symmetry breaking and take into account using flow equations effects of high energy QCD which influence the hadron scale physics.

2.2.2 Model calculations in QCD

Calculations made in the Coulomb gauge QCD illustrate clear the scheme of flow equations. The question we address is, how starting with canonical QCD Hamiltonian to obtain using flow equations an effective block-diagonal Hamiltonian with fixed number of Fock components in each block. It seems, that this goal is possible to achieve only for a 'confined QCD' with constituent quarks and gluons. Indeed, in the presence of a strong confining interaction current (bare) quarks and gluons are renormalized, getting dressed and becoming constituent quarks and gluons. This QCD motivated Hamiltonian can be written in a Fock space of constituent quarks q and gluons g as

$$H_{QCD}(q, g) = \left(\begin{array}{c|c|c} q\bar{q} & & \\ \hline & q\bar{q}g & \\ \hline & & gg \\ & & q\bar{q}q\bar{q} \end{array} \right), \quad (60)$$

where in every next Fock state a $q\bar{q}$ pair or a gluon are added. In terms of constituent quasiparticles, there is a natural energy gap of order of one GeV between different sectors. In the gauge field theories, mixing between sectors is mediated by minimally coupled gauge fields and is strongly suppressed. Small parameter is no longer the coupling constant, but rather a ratio of the off-diagonal matrix element which mixes sectors to the energy gap between diagonal sectors. In the canonical QCD, the off-diagonal sector is given by the mixing Coulomb interaction which value is of order of an inverse Bohr radius or a current quark mass – several MeV, and the mass gap between sectors is defined by a confining scale with a value of order of a constituent mass – one GeV; i.e. a small parameter is

$$\frac{V_{12}}{M_1 - M_2} \sim \frac{10MeV}{1GeV} \ll 1, \quad (61)$$

where V_{12} is a matrix element of canonical interaction between the first and second Fock state with masses M_1 and M_2 correspondingly. Thus, in the constituent basis, mixing between sectors is suppressed and can be eliminated perturbatively by flow equations with a small parameter given by Eq. (61). However, perturbative expansion in this parameter holds when working between sectors but not inside a diagonal sector where a strong confining interaction dominates. In the effective block-diagonal Hamiltonian, the diagonal sectors should be diagonalized numerically.

At low energies one could think about introducing hadron states as elementary degrees of freedom, and constructing a phenomenological Hamiltonian for strong interactions of the form

$$H_{strong}(hadron) = \left(\begin{array}{c|c|c} meson & & \\ \hline & hybrid & \\ \hline & & glueball \end{array} \right), \quad (62)$$

where hadron states are put on diagonal with increasing glue content from up-left corner to down-right; off-diagonal blocks (here empty cells) contain possible interactions which mix different diagonal blocks (Fock sectors). In order to find the physical (pure) states

one should block-diagonalize this Hamiltonian matrix, eliminating "off-diagonal" interactions. Probably, one could do it perturbatively, since as known from phenomenology the mixing between hadron Fock states is suppressed and a small parameter for iterative procedure could be

$$\frac{M(\text{hybrid}) - M(\text{meson})}{M(\text{hybrid})} \sim \frac{1}{10} \ll 1, \quad (63)$$

where $M(\text{hybrid})$ denotes hybrid mass, etc. This description is along with effective low-energy models of nuclear physics, where nucleons N are degrees of freedom and pions π are mediating interactions between them.

Summarizing, it seems that the 'confined' QCD provides an effective description which matches degrees of freedom in both Hamiltonians given by Eqs. (60) and (62). In this framework, using flow equations perturbatively we reduce bound state problem to an eigenstate equation with the lowest Fock component of quasiparticles.

2.2.3 Duality and BV transformation

Now that we know how to work with the 'confined' QCD which resembles CQM, the question is, how to get this effective theory. In other words, how to transform the original canonical QCD which is strong coupled, with nonfixed number of particles and has complex vacuum with confinement and chiral symmetry breaking to the CQM type effective theory which is weak coupled, where the valence quarks and gluons are confined in bound states, with the chiral symmetry dynamically broken, and has simple vacuum state. We are looking for a dual transformation between these two theories, in the sense that the duality is between the strong interacting QCD and weak interacting effective theory.

Many body approach suggests, that the BCS type Bogoliubov-Valatin (BV) transformation might fill the gap between QCD and CQM. We adopt that the BV transformed QCD has chiral invariant simple vacuum, but instead contains chiral noninvariant interactions including strong BCS interactions, which reflect confinement and the chiral symmetry breaking explicitly, and residual dynamical interactions, which are weak. Applying flow equations to the BV transformed 'confined' QCD, we eliminate off-diagonal dynamical interactions and obtain the block-diagonal effective Hamiltonian containing strong confining chiral noninvariant interactions in addition to dynamical interactions in each block. Diagonalizing sector Hamiltonians numerically, we obtain eigenstates which are confined and are not invariant under the chiral transformation, and involve dynamics. Due to the dynamical interactions, we obtain for the first time equations and corresponding solutions which are both UV and IR finite. Also, for the first time, solutions include explicitly confinement and chiral symmetry breaking as well as dynamically propagating gluons.

2.2.4 QCD motivated Hamiltonian in the Coulomb gauge

One of the ways to implement confining potential in the QCD Hamiltonian is to use the Coulomb gauge, which is defined as $\nabla \cdot A = 0$. The Coulomb gauge QCD Hamiltonian

includes the free Hamiltonian, H_0 , and two types of interactions: instantaneous, W , describing static properties, and dynamical, V , involving propagating gluons,

$$H = H_0 + W + V. \quad (64)$$

The free Hamiltonian (quark and gluon kinetic energies) is given by

$$\begin{aligned} H_0 &= \int d\mathbf{x} \psi^\dagger(\mathbf{x}) (-i\boldsymbol{\alpha} \cdot \boldsymbol{\nabla} + \beta m) \psi(\mathbf{x}) \\ &+ \text{Tr} \int d\mathbf{x} \left(\boldsymbol{\Pi}^2(\mathbf{x}) + \mathbf{B}_A^2(\mathbf{x}) \right), \end{aligned} \quad (65)$$

where the non-abelian magnetic field is $\mathbf{B} = B_i = \nabla_j A_k - \nabla_k A_j + g[A_j, A_k]$, and its abelian part is represented by \mathbf{B}_A . Dynamical interaction includes the minimal quark-gluon coupling, V_{qg} , and the non-abelian three- and four-gluon interactions, V_{gg} , i.e. $V = V_{qg} + V_{gg}$. Explicitly they are given by

$$\begin{aligned} V_{qg} &= -g \int d\mathbf{x} \psi^\dagger(\mathbf{x}) \boldsymbol{\alpha} \cdot \mathbf{A}(\mathbf{x}) \psi(\mathbf{x}) \\ V_{gg} &= \text{Tr} \int d\mathbf{x} \left(J\boldsymbol{\Pi}(\mathbf{x})J^{-1}\boldsymbol{\Pi}(\mathbf{x}) - \boldsymbol{\Pi}^2(\mathbf{x}) \right) + \text{Tr} \int d\mathbf{x} \left(\mathbf{B}^2(\mathbf{x}) - \mathbf{B}_A^2(\mathbf{x}) \right). \end{aligned} \quad (66)$$

The Coulomb gauge fixing produces the instantaneous quark-quark and gluon-gluon interactions,

$$W = \frac{1}{2}g^2 \int d\mathbf{x}d\mathbf{y} J^{-1}\rho^a(\mathbf{x}) \langle \mathbf{x}, a | (\boldsymbol{\nabla} \cdot \mathbf{D})^{-1} (-\nabla^2) (\boldsymbol{\nabla} \cdot \mathbf{D})^{-1} | \mathbf{y}, b \rangle J\rho^b(\mathbf{y}), \quad (67)$$

with the leading order Coulomb behavior, $1/\bar{q}^2$. Here, the charge density, ρ , contains both quark and gluon components, $\rho^a(\mathbf{x}) = \psi^\dagger(\mathbf{x})T^a\psi(\mathbf{x}) + f^{abc}\mathbf{A}^b(\mathbf{x}) \cdot \boldsymbol{\Pi}^c(\mathbf{x})$. A complete solution of the Coulomb gauge constraint equations is encoded in the Fadeev-Popov determinant, $J = \det(\boldsymbol{\nabla} \cdot \mathbf{D})$ with $\mathbf{D} = \boldsymbol{\nabla} - g\mathbf{A}$, which is unknown. We assume, that a nonperturbative solution of J produces the linear confining potential. Thus, we consider QCD motivated Hamiltonian, given by the Coulomb gauge canonical Hamiltonian with the instantaneous interaction including the Coulomb and linear confining potentials; i.e. $W \rightarrow W_0$,

$$\begin{aligned} W_0 &= -\frac{1}{2} \int d\mathbf{x}d\mathbf{y} \rho^a(\mathbf{x}) V_{L+C}(|\mathbf{x} - \mathbf{y}|) \rho^a(\mathbf{y}) \\ C_f V_{L+C}(r) &= \sigma r - C_f \frac{\alpha_s}{r}. \end{aligned} \quad (68)$$

This QCD motivated Hamiltonian defines our model, used for calculations of glueball and meson bound states and presented below.

2.2.5 Effective Hamiltonian for gluodynamics in the Coulomb gauge

In a pure gluodynamics, charge density contains only the gluon component. Following the same strategy as before, we represent physical fields, which are three gluon field, \vec{A} , and its conjugate momentum, $\vec{\Pi}$, in a second quantized form,

$$\begin{aligned} A_i^a(\mathbf{x}) &= \int \frac{d\mathbf{k}}{(2\pi)^3} \frac{1}{\sqrt{2\omega_{\mathbf{k}}}} [a_i^a(\mathbf{k}) + a_i^{a\dagger}(-\mathbf{k})] e^{i\mathbf{k}\mathbf{x}} \\ \Pi_i^a(\mathbf{x}) &= -i \int \frac{d\mathbf{k}}{(2\pi)^3} \sqrt{\frac{\omega_{\mathbf{k}}}{2}} [a_i^a(\mathbf{k}) - a_i^{a\dagger}(-\mathbf{k})] e^{i\mathbf{k}\mathbf{x}}. \end{aligned} \quad (69)$$

Since a confining potential has been introduced, a trivial perturbative vacuum does not insure minimum for the ground state. Ground state is shifted to some unknown nonperturbative state $|0\rangle_{NP}$. The annihilation operator is defined to annihilate in this vacuum, i.e. $a|0\rangle_{NP} = 0$; and creation operator acting on this vacuum produces quasiparticle (effective gluon) with unknown energy $\omega(\mathbf{k})$. Gluon energy $\omega(\mathbf{k})$ is kept as a trial parameter through out the calculations and is found variationally by minimizing the vacuum (ground) state energy. The canonical commutation relation is

$$[a_i^a(\mathbf{k}), a_j^{b\dagger}(\mathbf{k}')] = (2\pi)^3 \delta^{ab} \delta^{(3)}(\mathbf{k} - \mathbf{k}') D_{ij}(\mathbf{k}), \quad (70)$$

where the gluon operators $a_i^a(\mathbf{k}) = \sum_{\lambda=1,2} \epsilon_i(\mathbf{k}, \lambda) a^a(\mathbf{k}, \lambda)$ are transverse, i.e. $\mathbf{k} \cdot \mathbf{a}^a(\mathbf{k}) = \mathbf{k} \cdot \mathbf{a}^{a\dagger}(\mathbf{k}) = 0$; so that polarization sum is

$$D_{ij}(\mathbf{k}) = \sum_{\lambda=1,2} \epsilon_i(\mathbf{k}, \lambda) \epsilon_j(\mathbf{k}, \lambda) = \delta_{ij} - \hat{k}_i \hat{k}_j, \quad (71)$$

with the unit vector $\hat{k}_i = k_i/k$; and $k_i \cdot D_{ij}(\mathbf{k}) = 0$.

In a second quantized form, the Coulomb gauge Hamiltonian of gluodynamics contains the following terms; the gluon kinetic energy is given by

$$H_0(l) = \frac{1}{2} \int \frac{d\mathbf{k}}{(2\pi)^3} \left[\left(\frac{\mathbf{k}^2}{\omega(\mathbf{k}, l)} + \omega(\mathbf{k}, l) \right) a_i^{a\dagger}(\mathbf{k}) a_i^a(\mathbf{k}) + \left(\frac{\mathbf{k}^2}{\omega(\mathbf{k}, l)} - \omega(\mathbf{k}, l) \right) \frac{1}{2} (a_i^a(\mathbf{k}) a_i^a(-\mathbf{k}) + \text{h.c.}) \right]. \quad (72)$$

The instantaneous gluon-gluon interaction (Eq. (68)) is given by

$$H_{L+C} = -\frac{1}{8} f^{abc} f^{ade} \int \left(\prod_{n=1}^4 \frac{d\mathbf{k}_n}{(2\pi)^3} \right) (2\pi)^3 \delta^{(3)}(\sum_m \mathbf{k}_m) \left(\frac{\omega(\mathbf{k}_2, l) \omega(\mathbf{k}_4, l)}{\omega(\mathbf{k}_1, l) \omega(\mathbf{k}_3, l)} \right)^{1/2} \quad (73)$$

$$V_{L+C}(\mathbf{k}_1 + \mathbf{k}_2): [a_i^b(\mathbf{k}_1) + a_i^{b\dagger}(-\mathbf{k}_1)] [a_i^c(\mathbf{k}_2) - a_i^{c\dagger}(-\mathbf{k}_2)] [a_j^d(\mathbf{k}_3) + a_j^{d\dagger}(-\mathbf{k}_3)] [a_j^e(\mathbf{k}_4) - a_j^{e\dagger}(-\mathbf{k}_4)] :,$$

where $V_{L+C}(\mathbf{k})$ is a Fourier transform in the momentum space of linear confining plus Coulomb potentials,

$$V_{L+C} = 2\pi C_{adj} \frac{\alpha_s}{\mathbf{k}^2} + 4\pi \frac{\sigma_{adj}}{\mathbf{k}^4}, \quad (74)$$

here the adjoint Casimir is $C_{adj} = N_c$. The nonabelian gluon part (Eq. (66)) includes in the order $O(g)$ a triple-gluon coupling

$$H_{3g}(l) = \frac{i}{2\sqrt{2}} f^{abc} \int \left(\prod_{n=1}^3 \frac{d\mathbf{k}_n}{(2\pi)^3} \right) (2\pi)^3 \delta^{(3)}(\sum_m \mathbf{k}_m) \frac{\Gamma_{ijk}(\mathbf{k}_1, \mathbf{k}_2, \mathbf{k}_3)}{\sqrt{\omega(\mathbf{k}_1, l) \omega(\mathbf{k}_2, l) \omega(\mathbf{k}_3, l)}} \quad (75)$$

$$: [g_0(\mathbf{k}_1, \mathbf{k}_2, \mathbf{k}_3, l) a_i^a(\mathbf{k}_1) a_j^b(\mathbf{k}_2) a_i^c(\mathbf{k}_3) + \dots] :,$$

with

$$\Gamma_{ijk}(\mathbf{k}_1, \mathbf{k}_2, \mathbf{k}_3, l) = \frac{1}{6} ((k_1 - k_3)_j \delta_{ik} + (k_2 - k_1)_k \delta_{ij} + (k_3 - k_2)_i \delta_{jk}). \quad (76)$$

In the order $O(g^2)$ the normal-ordered four-gluon vertex reads

$$\begin{aligned}
H_{4g}(l) &= \frac{\alpha_s \pi}{4} f^{abc} f^{ade} \int \left(\prod_{n=1}^4 \frac{d\mathbf{k}_n}{(2\pi)^3} \right) (2\pi)^3 \delta^{(3)}(\sum_m \mathbf{k}_m) \\
&\quad \frac{1}{\sqrt{\omega(\mathbf{k}_1, l)\omega(\mathbf{k}_2, l)\omega(\mathbf{k}_3, l)\omega(\mathbf{k}_4, l)}} \\
&\quad : [a_i^b(\mathbf{k}_1) + a_i^{b\dagger}(-\mathbf{k}_1)] [a_j^c(\mathbf{k}_2) + a_j^{c\dagger}(-\mathbf{k}_2)] [a_i^d(\mathbf{k}_3) + a_i^{d\dagger}(-\mathbf{k}_3)] [a_j^e(\mathbf{k}_4) + a_j^{e\dagger}(-\mathbf{k}_4)] : .
\end{aligned} \tag{77}$$

Coupling constants and masses (relevant and marginal operators, respectively) are functions of the flow parameter l and momenta involved. In addition terms from normal ordering with respect to the NP vacuum $|0\rangle_{NP}$ arise; condensates O_0 , O_{L+C} , O_{4g} and gluon polarization operators Π_{L+C} , Π_{4g} .

Hamiltonian matrix of gluodynamics is depicted in the Table 3. It includes the triple-gluon vertex (for example, element H_{14}) and the instantaneous gluon-gluon interaction (for example, element H_{15}); (four-gluon vertex is not depicted). Off-diagonal elements mixing different Fock sectors are eliminated by flow equations.

Elimination of the off-diagonal elements through the second order generates the Hamiltonian matrix depicted in the Table 4. Explicit form of the effective Hamiltonian is not given here (for details see [3]). Black area in the effective gg interaction (H_{33}^{eff}) depicts the interaction generated by flow equations.

We solve the effective Hamiltonian in the two lowest sectors. This gives the gap equation and the Bethe-Salpeter bound equation for the glueball states.

Minimizing the ground state energy (H_{11}^{eff}),

$$\frac{\delta \langle 0 | H_{\text{eff}} | 0 \rangle}{\delta \omega_{\mathbf{k}}} = 0, \tag{78}$$

we obtain the gap equation for the effective gluon energy, $\omega(\mathbf{k})$, which is a function of gluon momentum \mathbf{k} and the cut-off Λ . Gap equation can be also obtained by demanding the off-diagonal one-body operator (H_{13}^{eff}), having the structure $(aa + a^\dagger a^\dagger)$, to be equal to zero (thus it is not depicted in the Table 4). Explicitly the gap equation is given by

$$\begin{aligned}
\omega_{\mathbf{k}}^2 &= k^2 + m_{CT}^2(\Lambda) \\
&+ \frac{1}{4} N_c \int \frac{d\mathbf{q}}{(2\pi)^3} \frac{1}{\omega_{\mathbf{q}}} V_{L+C}(\mathbf{k} - \mathbf{q}) \left(1 + (\hat{k}\hat{q})^2 \right) (\omega_{\mathbf{q}}^2 - \omega_{\mathbf{k}}^2) e^{-q^2/\Lambda^2} \\
&+ \alpha_s \pi N_c \int \frac{d\mathbf{q}}{(2\pi)^3} \frac{1}{\omega_{\mathbf{q}}} \left(3 - (\hat{k}\hat{q})^2 \right) e^{-q^2/\Lambda^2} \\
&- 2\alpha_s \pi N_c \int \frac{d\mathbf{q}}{(2\pi)^3} \frac{1}{\omega_{\mathbf{q}} \omega_{\mathbf{k}-\mathbf{q}} \omega_{\mathbf{q}} + \omega_{\mathbf{k}-\mathbf{q}}} G(\mathbf{k}, \mathbf{q}) e^{-4q^2/\Lambda^2},
\end{aligned} \tag{79}$$

where the mass counterterm $m_{CT}(\Lambda)$ is defined by

$$m_{CT}^2(\Lambda) = -\frac{\alpha_s}{\pi} N_c \frac{11}{6} \Lambda^2, \tag{80}$$

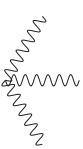
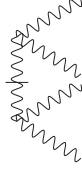
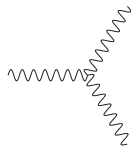
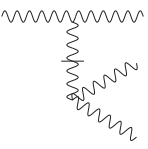
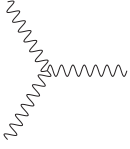
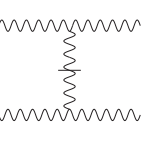

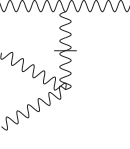

	$ 0\rangle$	$ g\rangle$	$gg\rangle$	$ ggg\rangle$	$ gggg\rangle$
$ 0\rangle$					
$ g\rangle$					
$ gg\rangle$					
$ ggg\rangle$					
$ gggg\rangle$					

Table 3: Hamiltonian of gluodynamics in the Coulomb gauge.

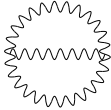

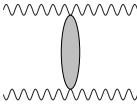
	$ 0\rangle$	$ g\rangle$	$gg\rangle$	$ ggg\rangle$	$ gggg\rangle$
$ 0\rangle$					
$ g\rangle$					
$ gg\rangle$					
$ ggg\rangle$					
$ gggg\rangle$					

Table 4: Effective Hamiltonian of gluodynamics generated through the second order by flow equations in the Coulomb gauge.

which absorbs the leading ultraviolet divergences in H_{eff} as $\Lambda \rightarrow \infty$. In the regulating fuction, we assume all external momenta to be soft compared to momentum flowing in the loop. Here, the tensor structure of generated terms is given by

$$G(\mathbf{k}, \mathbf{q}) = 2(1 - (\hat{k}\hat{q})^2) \left(k^2 + q^2 + \frac{k^2 q^2}{2(\mathbf{k} - \mathbf{q})^2} (1 + (\hat{k}\hat{q})^2) \right), \quad (81)$$

and V_{L+C} is the Fourier transform of the sum of linear and Coulomb potentials. The obtained gluon gap equation is both UV and IR finite. UV divergent behavior arising from the Coulomb interaction, four-gluon, and dynamically generated terms is cancelled by the canonical gluon mass counterterm.

We approximate a glueball bound state to consist of two valence constituent gluons. The glueball wave function in the rest frame is

$$|\psi_n\rangle = \int \frac{d\mathbf{q}}{(2\pi)^3} \phi_n^{ij}(\mathbf{q}) a_i^{a\dagger}(\mathbf{q}) a_j^{a\dagger}(-\mathbf{q}) |0\rangle_{NP}, \quad (82)$$

where $a^\dagger(\mathbf{q})$ creates a quasiparticle from a nontrivial vacuum $|0\rangle_{NP}$ with an effective dispersion relation $\omega(\mathbf{q})$. Since in this constituent basis an effective Hamiltonian H_{eff} is block-diagonal, the mixing with four gluon and higher states is suppressed. Therefore Tamm-Dancoff approach with H_{eff} is a reasonable approximaion for bound states. To obtain the Tamm-Dancoff bound state equation we project the Schrödinger equation $H_{eff}|\psi_n\rangle = E_n|\psi_n\rangle$ on the two-body sector; the result reads

$$\langle \psi_n | [H_{eff}, a^{i\dagger}(\mathbf{q}) a^{j\dagger}(-\mathbf{q})] | 0 \rangle = (E_n - E_0) \left(X_{i'j'}^{ij}(\mathbf{q}) \phi_n^{i'j'}(\mathbf{q}) \right), \quad (83)$$

with the notation

$$\left(X_{i'j'}^{ij}(\mathbf{q}) \phi_n^{i'j'}(\mathbf{q}) \right) = D_{ii'}(\mathbf{q}) D_{jj'}(\mathbf{q}) \phi_n^{i'j'}(\mathbf{q}) + D_{ij'}(\mathbf{q}) D_{ji'}(\mathbf{q}) \phi_n^{i'j'}(-\mathbf{q}), \quad (84)$$

here color indices are omitted, the polarization sum D_{ij} is given in Eq.(71), and H_{eff} is given in the Table 4. In Eq. (83) we subtracted the vacuum energy E_0 , defined as $H_{eff}|0\rangle_{NP} = E_0|0\rangle_{NP}$. Explicitly Tamm-Dancoff equation for scalar and pseudoscalar glueball states with total angular momentum J , parity P , and charge conjugation C and only the instantaneous interactions included is given by

$$\begin{aligned} M_n \phi_n(q) &= \left[\left(\frac{q^2 + \tilde{m}_{CT}^2(\Lambda)}{\omega(\mathbf{q})} + \omega(\mathbf{q}) \right) \right. \\ &+ \frac{1}{4} N_c \int \frac{d\mathbf{p}}{(2\pi)^3} V_{L+C}(\mathbf{p} - \mathbf{q}) \left(1 + (\hat{p}\hat{q})^2 \right) \frac{\omega^2(\mathbf{p}) + \omega^2(\mathbf{q})}{\omega(\mathbf{p})\omega(\mathbf{q})} e^{-p^2/\Lambda^2} \left. \right] \phi_n(q) \\ &- \frac{1}{8} N_c \int \frac{d\mathbf{p}}{(2\pi)^3} V_{L+C}(\mathbf{p} - \mathbf{q}) \frac{(\omega(\mathbf{p}) + \omega(\mathbf{q}))^2}{\omega(\mathbf{p})\omega(\mathbf{q})} F^{JPC}(\mathbf{p}, \mathbf{q}) \phi_n(p), \end{aligned} \quad (85)$$

with

$$\begin{aligned} F^{0++}(\mathbf{p}, \mathbf{q}) &= 1 + (\hat{p}\hat{q})^2 \\ F^{0-+}(\mathbf{p}, \mathbf{q}) &= 2(\hat{p}\hat{q}). \end{aligned} \quad (86)$$

Here the Coulomb mass counterterm is given by

$$\widetilde{m}_{CT}^2(\Lambda) = -\frac{\alpha_s N_c}{\pi} \frac{N_c}{3} \Lambda^2, \quad (87)$$

and V_{L+C} is the sum of linear and Coulomb potentials in the momentum space. One-body sector of the effective Hamiltonian contributes to the kinetic part of the Tamm-Dancoff equation, and two-body effective interaction to the potential part. UV divergences, coming from the Coulomb potential, are cancelled by the mass counterterm. IR divergent behavior, due to the confining potential, cancels in the potential and kinetic parts with each other. Such complete cancelation happens only for the color-singlet state, and does not occur for colored objects.

For completeness, we summarize the complete Tamm-Dancoff equation in the scalar and pseudoscalar channels when all the terms up to the second order (instantaneous, four-gluon and dynamical interactions) are included. It is given by

$$\begin{aligned} (E_n - E_0)\phi_n(q) = & \left[\left(\frac{q^2 + m_{CT}^2(\Lambda)}{\omega_{\mathbf{q}}} + \omega_{\mathbf{q}} \right) \right. \\ & + \frac{1}{4} N_c \int \frac{d\mathbf{p}}{(2\pi)^3} V_{L+C}(\mathbf{p} - \mathbf{q}) \left(1 + (\hat{p}\hat{q})^2 \right) \frac{\omega_{\mathbf{p}}^2 + \omega_{\mathbf{q}}^2}{\omega_{\mathbf{p}}\omega_{\mathbf{q}}} e^{-p^2/\Lambda^2} \\ & + \alpha_s \pi N_c \int \frac{d\mathbf{p}}{(2\pi)^3} \frac{1}{\omega_{\mathbf{p}}\omega_{\mathbf{q}}} \left(3 - (\hat{p}\hat{q})^2 \right) e^{-p^2/\Lambda^2} \\ & \left. - \alpha_s \pi N_c \int \frac{d\mathbf{p}}{(2\pi)^3} \frac{1}{\omega_{\mathbf{p}}\omega_{\mathbf{q}}\omega_{\mathbf{p}-\mathbf{q}}} \frac{G(\mathbf{p}, \mathbf{q})}{\omega_{\mathbf{p}} + \omega_{\mathbf{p}-\mathbf{q}}} e^{-4p^2/\Lambda^2} \right] \phi_n(q) \\ & + \left[-\frac{1}{8} N_c \int \frac{d\mathbf{p}}{(2\pi)^3} V_{L+C}(\mathbf{p} - \mathbf{q}) \frac{(\omega_{\mathbf{p}} + \omega_{\mathbf{q}})^2}{\omega_{\mathbf{p}}\omega_{\mathbf{q}}} F^{JPC}(\mathbf{p}, \mathbf{q}) \phi_n(p) \right. \\ & + \alpha_s \pi N_c \int \frac{d\mathbf{p}}{(2\pi)^3} \frac{1}{2\omega_{\mathbf{p}}\omega_{\mathbf{q}}} \left(3 - (\hat{p}\hat{q})^2 \right) E^{JPC}(\mathbf{p}, \mathbf{q}) \phi_n(p) \\ & \left. + \alpha_s 2\pi N_c \int \frac{d\mathbf{p}}{(2\pi)^3} \frac{1}{\omega_{\mathbf{p}}\omega_{\mathbf{q}}} \frac{D^{JPC}(\mathbf{p}, \mathbf{q})}{\omega_{\mathbf{p}-\mathbf{q}}^2} \left(1 - \frac{(\omega_{\mathbf{k}} - \omega_{\mathbf{q}})^2}{(\omega_{\mathbf{k}} - \omega_{\mathbf{q}})^2 + \omega_{\mathbf{k}-\mathbf{q}}^2} \right) \phi_n(p) \right], \quad (88) \end{aligned}$$

with the total angular momentum J , parity P , and charge conjugation C . Here the tensor structures are given by

$$\begin{aligned} F^{0++}(\mathbf{p}, \mathbf{q}) &= 1 + (\hat{p}\hat{q})^2 \\ F^{0-+}(\mathbf{p}, \mathbf{q}) &= 2(\hat{p}\hat{q}) \\ E^{0++}(\mathbf{p}, \mathbf{q}) &= 1 \\ E^{0-+}(\mathbf{p}, \mathbf{q}) &= 0 \\ D^{0++}(\mathbf{p}, \mathbf{q}) &= G(\mathbf{p}, \mathbf{q}) = 2(1 - (\hat{p}\hat{q})^2) \left(p^2 + q^2 + \frac{p^2 q^2}{2(\mathbf{p} - \mathbf{q})^2} (1 + (\hat{p}\hat{q})^2) \right) \\ D^{0-+}(\mathbf{p}, \mathbf{q}) &= 2p^2 q^2 (1 - (\hat{p}\hat{q})^2) \left(\frac{2}{pq} + \frac{1}{(\mathbf{p} - \mathbf{q})^2} (\hat{p}\hat{q}) \right). \quad (89) \end{aligned}$$

Again, this equation is both UV and IR finite.

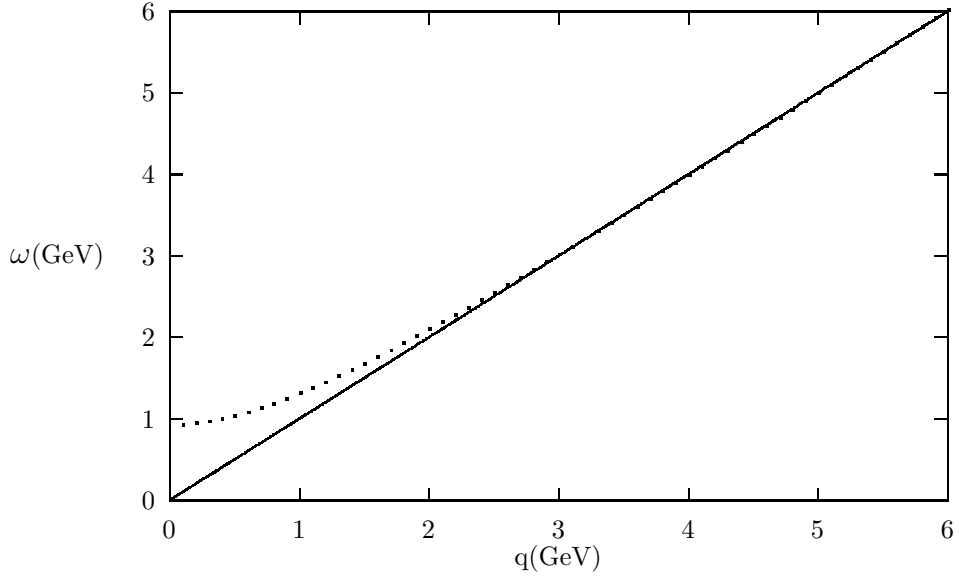


Figure 8: One particle dispersion relation. Dots represent the numerical solution of gap equation $\omega(\mathbf{k})$ ($\alpha_s = 0.4, \sigma = 0.18\text{GeV}^2, \Lambda = 4\text{GeV}, N_c = 3$), the solid line stays for the free dispersion relation $\omega(\mathbf{k}) = k$.

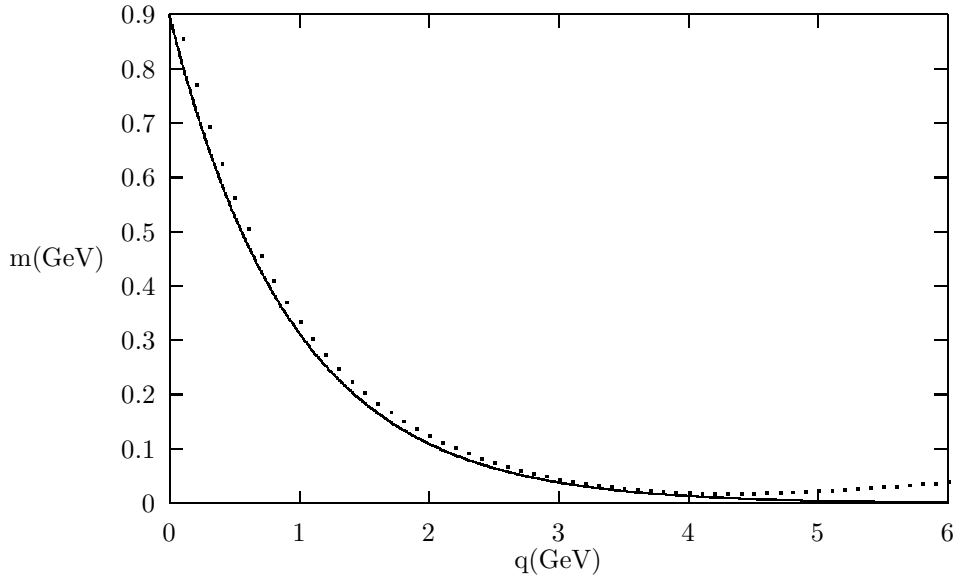


Figure 9: Gluon mass. Dots represent the numerical solution for $m(\mathbf{k}) = \omega(\mathbf{k}) - k$ ($\alpha_s = 0.4, \sigma = 0.18\text{GeV}^2, \Lambda = 4\text{GeV}, N_c = 3$), the solid line is a fit $m(\mathbf{k}) = 0.9 * \exp(-k/0.95)$ (parameters are in GeV).

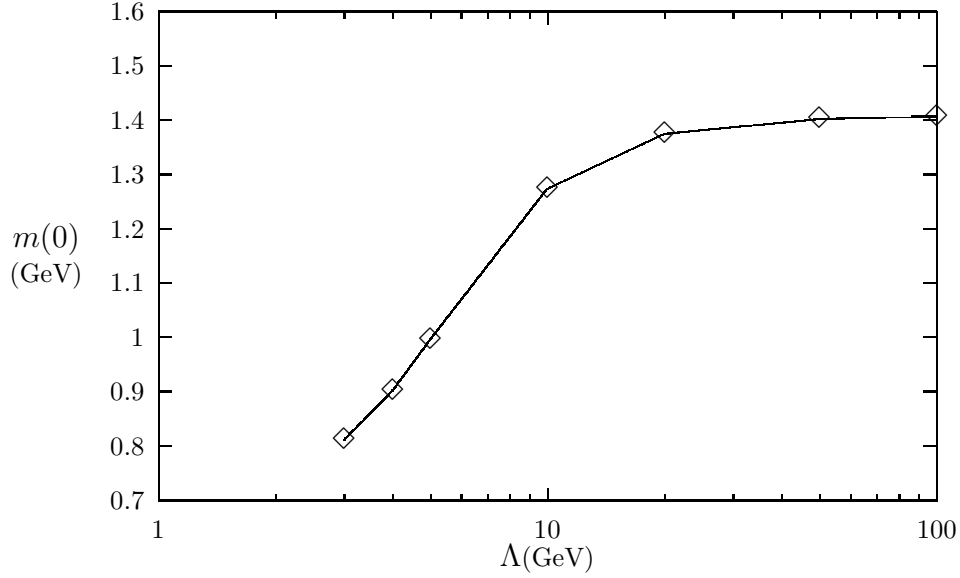


Figure 10: Cut-off dependence of the effective gluon mass ($\alpha_s = 0.4$, $\sigma = 0.18\text{GeV}^2$, $N_c = 3$).

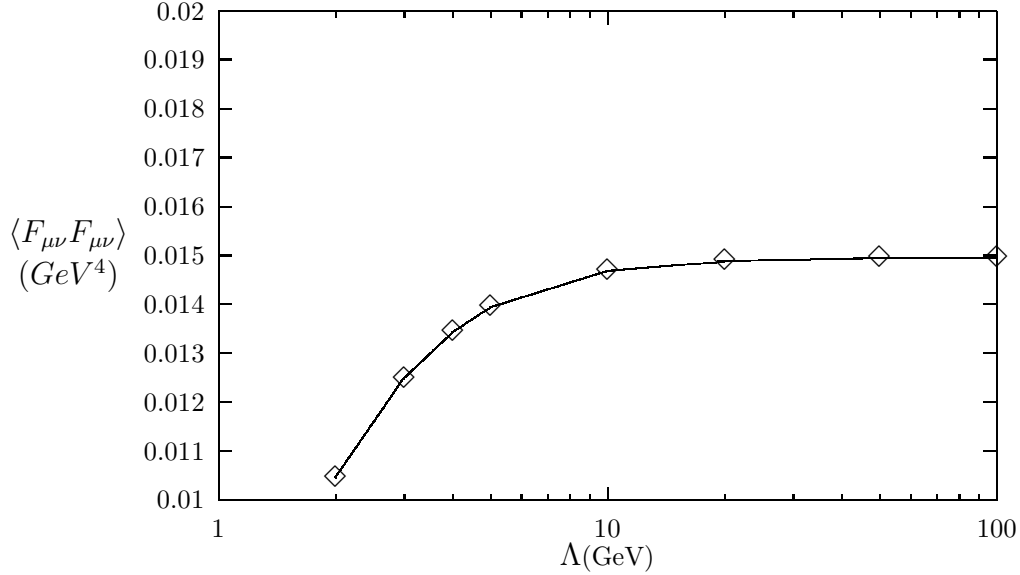


Figure 11: Gluon condensate ($\alpha_s = 0.4$, $\sigma = 0.18\text{GeV}^2$, $N_c = 3$).

Numerical results

Numerical solution of the gap equation is shown on Figure 8, with dots for numerics, solid line is a perturbative free behavior, $\omega = k$. At large momenta an effective gluon energy covers the perturbative behavior, while at small momenta ω tends to a constant,

an effective gluon mass at zero momentum. We obtain $m(0) = 0.9 \text{ GeV}$ with the string tension $\sigma = 0.2 \text{ GeV}^2$. We define an effective gluon mass as the difference of the effective gluon energy and the perturbative value, Figure 9 (dots is numerics, solid line is a parametrization with an exponential fall off). At large momenta, there is zero mass and at $q \sim 0$ we have $m(0) \sim 1 \text{ GeV}$.

Effective gluon mass at zero gluon momentum as a function of the cut-off is given at Figure 10 (in logarithmic scale). Leading Λ^2 behavior is absorbed by the mass counterterm. The logarithmic dependence is left, which is relatively slow.

Gluon condensate, calculated using the numerically obtained gluon energy, is another nonperturbative characteristic. It grows as a function of Λ logarithmically (Fig. 11). We attribute this slow dependence to a numerical artefact. We regulate the gluon condensate by subtracting the perturbative contribution

$$\langle \frac{\alpha_s}{\pi} F_{\mu\nu}^a F_{\mu\nu}^a \rangle = \frac{N_c^2 - 1}{\pi^3} \int_0^\infty dk k^2 \alpha_s \frac{(\omega(\mathbf{k}) - k)^2}{2\omega(\mathbf{k})}. \quad (90)$$

Using the dispersion relation obtained above $\omega(\mathbf{k})$ the gluon condensate is obtained $1.3 \cdot 10^{-2} \text{ GeV}^4$ (for the cut-off $\Lambda = 4 \text{ GeV}$), that agrees with the sum rules. (Therefore $\Lambda = 4 \text{ GeV}$ has been used for all our numerical calculations.)

Numerical calculations of the Tamm-Dancoff equation, Eq.(85), are performed variationally with a set of gaussian test functions. Results of calculations for the lowest glueball states are presented in the Table (5) and compared with the available lattice data.

J^{PC}	0^{++}	0^{*++}	0^{-+}	0^{*-+}
Tamm-Dancoff, (MeV)	1760	2697	2142	2895
lattice data, (MeV)	1730(80)	2670(130)	2590(130)	3640(180)

Table 5: Glueball spectrum for the lowest scalar and pseudoscalar states ($\alpha_s = 0.4, \sigma = 0.18 \text{ GeV}^2, \Lambda = 4 \text{ GeV}, N_c = 3$). Lattice data are from C. Morningstar and M. Peardon, hep-lat/9901004.

Lattice calculations are done for $SU(3)$ pure gluodynamics, using anisotropic lattice and improved SII action. Better agreement with the lattice data is achieved for the scalar channel. Remarkable, the mass of the lowest scalar glueball 0^{++} is roughly twice of the effective gluon mass $m(0)$ obtained before. This confirms the constituent picture. The better agreement is achieved for the scalar masses, indicating that dynamical terms are important for the excited states and the complete Tamm-Dancoff equation with all terms should be solved.

2.2.6 Effective Hamiltonian for QCD in the Coulomb gauge

This model is also suitable to study the chiral symmetry breaking. Now, quarks are dynamical and the charge density has only the quark component. The instantaneous interaction contains the Coulomb plus linear confining potentials. Gluons are perturbative and quarks have unknown dispersion relation, dynamical energy $E(\mathbf{k})$ which is

parametrized through the BV angle $\Phi(\mathbf{k})$. Vacuum $|\Omega\rangle$ contains condensates of quark pairs (i.e. it is the BCS vacuum). The Fock space is constructed from this vacuum using quasiparticle operators b^\dagger and d^\dagger which appear in the field expansions

$$\begin{aligned}\psi(\mathbf{x}) &= \sum_s \int \frac{d\mathbf{k}}{(2\pi)^3} [u(\mathbf{k}, s)b(\mathbf{k}, s) + v(-\mathbf{k}, s)d^\dagger(-\mathbf{k}, s)]e^{i\mathbf{k}\mathbf{x}} \\ \mathbf{A}(\mathbf{x}) &= \sum_a \int \frac{d\mathbf{k}}{(2\pi)^3} \frac{1}{\sqrt{2\omega(\mathbf{k})}} [a(\mathbf{k}, a) + a^\dagger(-\mathbf{k}, a)]e^{i\mathbf{k}\mathbf{x}} \\ \mathbf{\Pi}(\mathbf{x}) &= -i \sum_a \int \frac{d\mathbf{k}}{(2\pi)^3} \sqrt{\frac{\omega(\mathbf{k})}{2}} [a(\mathbf{k}, a) - a^\dagger(-\mathbf{k}, a)]e^{i\mathbf{k}\mathbf{x}},\end{aligned}\tag{91}$$

with $b|\Omega\rangle = d|\Omega\rangle = 0$. Here the quark operators are given in the helicity basis and all discrete numbers (helicity, color, and flavor for the quarks and color for the gluons) are collectively denoted by s and a , respectively. We use spinors in the massive basis, where nonzero effective quark mass explicitly is included in the spinor

$$\begin{aligned}u(\mathbf{k}, s) &= \sqrt{E(\mathbf{k}) + M(\mathbf{k})} \begin{pmatrix} 1 \\ \boldsymbol{\sigma} \cdot \mathbf{k} / (E(\mathbf{k}) + M(\mathbf{k})) \end{pmatrix} \chi_s \\ &= \frac{1}{\sqrt{2}} \begin{pmatrix} \sqrt{1 + s(\mathbf{k})} \chi_s \\ \sqrt{1 - s(\mathbf{k})} (\boldsymbol{\sigma} \cdot \hat{\mathbf{k}}) \chi_s \end{pmatrix} \\ v(-\mathbf{k}, s) &= \sqrt{E(\mathbf{k}) + M(\mathbf{k})} \begin{pmatrix} -\boldsymbol{\sigma} \cdot \mathbf{k} / (E(\mathbf{k}) + M(\mathbf{k})) \\ 1 \end{pmatrix} (-i\sigma_2 \chi_s) \\ &= \frac{1}{\sqrt{2}} \begin{pmatrix} -\sqrt{1 - s(\mathbf{k})} (\boldsymbol{\sigma} \cdot \hat{\mathbf{k}}) (-i\sigma_2 \chi_s) \\ \sqrt{1 + s(\mathbf{k})} (-i\sigma_2 \chi_s) \end{pmatrix},\end{aligned}\tag{92}$$

with sine and cosine of the Bogoliubov angle $\Phi(\mathbf{k})$ given by

$$\begin{aligned}\sin(\Phi(\mathbf{k})) &= s(\mathbf{k}) = \frac{M(\mathbf{k})}{\sqrt{\mathbf{k}^2 + M^2(\mathbf{k})}}, \quad \cos(\Phi(\mathbf{k})) = c(\mathbf{k}) = \frac{k}{\sqrt{\mathbf{k}^2 + M^2(\mathbf{k})}} \\ E(\mathbf{k}) &= \sqrt{\mathbf{k}^2 + M^2(\mathbf{k})},\end{aligned}\tag{93}$$

$E(\mathbf{k})$ is a single-quark energy which we refer as a gap energy below. Effective quark mass $M(\mathbf{k})$ is kept as an unknown variational parameter through out the calculations, and is found from the gap equation by minimizing the ground state (vacuum) energy. Gluon energy is $\omega(\mathbf{k}) = k$.

With the definition Eq. (92), the spinors satisfy the nonrelativistic normalization and orthogonality relations $u^\dagger(\mathbf{k}, s)u(\mathbf{k}, s) = v^\dagger(-\mathbf{k}, s)v(-\mathbf{k}, s) = 1$ and $u^\dagger(\mathbf{k}, s)v(-\mathbf{k}, s) = v^\dagger(-\mathbf{k}, s)u(\mathbf{k}, s) = 0$. Canonical (anti)commutation relations are

$$\begin{aligned}\{b(\mathbf{k}, s), b^\dagger(\mathbf{k}', s')\} &= \{d(-\mathbf{k}, s), d^\dagger(-\mathbf{k}', s')\} = (2\pi)^3 \delta(\mathbf{k} - \mathbf{k}') \delta_{s, s'} \\ [a_i(\mathbf{k}, a), a_j^\dagger(\mathbf{k}', a')] &= (2\pi)^3 \delta(\mathbf{k} - \mathbf{k}') D_{ij}(\mathbf{k}) \delta_{a, a'},\end{aligned}\tag{94}$$

where the gluon operators $\mathbf{a} = a_i(\mathbf{k})^a = \sum_{\lambda=1,2} \epsilon_i(\mathbf{k}, \lambda) a^a(\mathbf{k}, \lambda)$ are transverse, i.e. $\mathbf{k} \cdot \mathbf{a}^a(\mathbf{k}) = \mathbf{k} \cdot \mathbf{a}^{a\dagger}(\mathbf{k}) = 0$, and $D_{ij}(\mathbf{k})$ is a polarization sum

$$D_{ij}(\mathbf{k}) = \sum_{\lambda=1,2} \epsilon_i(\mathbf{k}, \lambda) \epsilon_j(\mathbf{k}, \lambda) = \delta_{ij} - \hat{k}_i \hat{k}_j, \quad (95)$$

with unit vector component $\hat{k}_i = k_i/|\mathbf{k}|$ and $\hat{k}_i \cdot D_{ij}(\mathbf{k}) = 0$.

Following the same scheme, we represent the Hamiltonian in a second quantized form. The free Hamiltonian (kinetic quark and gluon energies) is given by

$$\begin{aligned} H_0(l) &= \sum_s \int \frac{d\mathbf{k}}{(2\pi)^3} \left((kc(\mathbf{k}, l) + ms(\mathbf{k}, l)) [b_s^\dagger(\mathbf{k}) b_s(\mathbf{k}) + d_s^\dagger(\mathbf{k}) d_s(\mathbf{k})] \right. \\ &+ (ks(\mathbf{k}, l) - mc(\mathbf{k}, l)) [b_s^\dagger(\mathbf{k}) d_s^\dagger(-\mathbf{k}) + d_s(-\mathbf{k}) b_s(\mathbf{k})] \\ &+ \left. \sum_a \int \frac{d\mathbf{k}}{(2\pi)^3} \omega(\mathbf{k}) a_i^{a\dagger}(\mathbf{k}) a_i^a(\mathbf{k}) \right). \end{aligned} \quad (96)$$

The quark-gluon vertex is given by

$$H_{qg}(l) = - \sum_{s_1, s_2, a} \int \left(\prod_{n=1}^3 \frac{d\mathbf{k}_n}{(2\pi)^3} \right) \left[g_0(\mathbf{k}_1, \mathbf{k}_2, \mathbf{k}_3, l) d_{s_1}(-\mathbf{k}_1) T^a b_{s_2}(\mathbf{k}_2) \frac{a_i^a(\mathbf{k}_3)}{\sqrt{2\omega(\mathbf{k}_3)}} \right. \quad (97)$$

$$\left. v_{s_1}^\dagger(-\mathbf{k}_1) \alpha_i u_{s_2}(\mathbf{k}_2) (2\pi)^3 \delta^{(3)}(\mathbf{k}_1 - \mathbf{k}_2 - \mathbf{k}_3) + \dots \right], \quad (98)$$

where $E(\mathbf{k}) = \sqrt{\mathbf{k}^2 + M^2(\mathbf{k})}$ and $\omega(\mathbf{k}) = k$. By implementing flow equations effective coupling constants are generated ($g_0(\mathbf{k}_1, \mathbf{k}_2, \mathbf{k}_3; l) \dots$) which are functions of all three momenta corresponding to a given Fock sector and depend upon the flow parameter l . The instantaneous interaction includes the linear confining and Coulomb potentials and is given in the quark sector by

$$\begin{aligned} H_{L+C}(l) &= \sum_{s_1 \dots s_4} \int \left(\prod_{n=1}^4 \frac{d\mathbf{k}_n}{(2\pi)^3} \right) (2\pi)^3 \delta^{(3)}(\mathbf{k}_1 + \mathbf{k}_3 - \mathbf{k}_2 - \mathbf{k}_4) V_{L+C}(\mathbf{k}_1, \mathbf{k}_2) \\ &: [u_{s_1}^\dagger(\mathbf{k}_1) b_{s_1}^\dagger(\mathbf{k}_1) + v_{s_1}^\dagger(-\mathbf{k}_1) d_{s_1}(-\mathbf{k}_1)] T^a [u_{s_2}(\mathbf{k}_2) b_{s_2}(\mathbf{k}_2) + v_{s_2}(-\mathbf{k}_2) d_{s_2}^\dagger(-\mathbf{k}_2)] \\ &[u_{s_3}^\dagger(\mathbf{k}_3) b_{s_3}^\dagger(\mathbf{k}_3) + v_{s_3}^\dagger(-\mathbf{k}_3) d_{s_3}(-\mathbf{k}_3)] T^a [u_{s_4}(\mathbf{k}_4) b_{s_4}(\mathbf{k}_4) + v_{s_4}(-\mathbf{k}_4) d_{s_4}^\dagger(-\mathbf{k}_4)] : , \end{aligned} \quad (99)$$

where $V_{L+C}(\mathbf{k}, \mathbf{q}) \rightarrow V_{L+C}(\mathbf{k} - \mathbf{q})$,

$$C_f V_{L+C}(\mathbf{k}) = 2\pi C_f \frac{\alpha_s}{\mathbf{k}^2} + 4\pi \frac{\sigma}{\mathbf{k}^4}, \quad (100)$$

with the fundamental Casimir operator $C_f = T^a T^a = (N_c^2 - 1)/2N_c = 4/3$. The spinors are also functions of the flow parameter, i.e. everywhere $u_s(\mathbf{k}, l)$ and $v_s(\mathbf{k}, l)$. In addition, the condensate O_0 , O_{L+C} and self-energy terms Σ_{L+C} arise due to the normal-ordering of the canonical QCD Hamiltonian with respect to the BCS vacuum. Dynamical quark

	$ 0\rangle$	$ q\rangle$	$ q\bar{q}\rangle$	$ q\bar{q}g\rangle$	$ q\bar{q}q\bar{q}\rangle$
$ 0\rangle$					
$ q\rangle$					
$ q\bar{q}\rangle$					
$ q\bar{q}g\rangle$					
$ q\bar{q}q\bar{q}\rangle$					

Table 6: QCD Hamiltonian in the Coulomb gauge.

energy is expressed through the BV angle, which is kept as a trial parameter through calculations.

Matrix elements of the Coulomb gauge normal-ordered Hamiltonian are shown in the Table 6. For example the quark-gluon coupling is given by the element H_{14} and the instantaneous interaction is given by H_{33} . Off-diagonal elements are eliminated by flow equations.

As a result of this elimination new terms arise in the diagonal sector, depicted in the Table 7.

The gap equation allows determination of a nontrivial vacuum with quark condensates and propagating quasiparticles, here quarks with a dynamical mass. There are several ways to obtain this equation, the most common based upon a variational principle to minimize the vacuum (ground state) energy. The variational parameter is the angle of transformation from undressed to dressed particle (quasiparticle) operators, $\Phi(\mathbf{k})$, which defines a quasiparticle basis (Eqs. (91) and (92)) with a dynamical quark mass $M(\mathbf{k})$. Therefore, analogously to the gluon sector, minimizing the vacuum energy of the effective

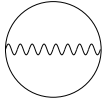
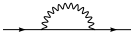
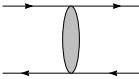
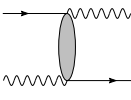
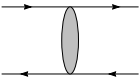
	$ 0\rangle$	$ q\rangle$	$ q\bar{q}\rangle$	$ q\bar{q}g\rangle$	$ q\bar{q}q\bar{q}\rangle$
$ 0\rangle$					
$ q\rangle$					
$ q\bar{q}\rangle$					
$ q\bar{q}g\rangle$					
$ q\bar{q}q\bar{q}\rangle$					

Table 7: Effective QCD Hamiltonian generated through the second order by flow equations in the Coulomb gauge.

Hamiltonian,

$$\frac{\delta\langle\Omega|H_{eff}|\Omega\rangle}{\delta\Phi(\mathbf{k})} = 0, \quad (101)$$

we obtain the gap equation for the unknown $\Phi(\mathbf{k})$ or $M(\mathbf{k})$. Using the condensate terms given by H_{11}^{eff} , the gap equation is obtained as

$$\begin{aligned} ks(\mathbf{k}) - m(\Lambda)c(\mathbf{k}) &= \int \frac{d\mathbf{q}}{(2\pi)^3} C_f V_{L+C}(\mathbf{k}, \mathbf{q}) \left[c(\mathbf{k})s(\mathbf{q}) - s(\mathbf{k})c(\mathbf{q})\hat{\mathbf{k}} \cdot \hat{\mathbf{q}} \right] e^{-q^2/\Lambda^2} \\ &+ \int \frac{d\mathbf{q}}{(2\pi)^3} C_f W(\mathbf{k}, \mathbf{q}) \left[c(\mathbf{k})s(\mathbf{q}) - s(\mathbf{k})c(\mathbf{q})\hat{\mathbf{k}} \cdot \hat{\mathbf{l}}\hat{\mathbf{q}} \cdot \hat{\mathbf{l}} \right] e^{-4q^2/(10^2)} \end{aligned}$$

where $\mathbf{l} = \mathbf{k} - \mathbf{q}$, the potential functions are given by

$$\begin{aligned} C_f V_{L+C}(\mathbf{k}, \mathbf{q}) &= \frac{1}{2} \frac{C_f g^2}{(\mathbf{k} - \mathbf{q})^2} + \frac{4\pi\sigma}{(\mathbf{k} - \mathbf{q})^4} \\ C_f W(\mathbf{k}, \mathbf{q}) &= \frac{C_f g^2}{\omega(\mathbf{k} - \mathbf{q})(E(\mathbf{q}) + \omega(\mathbf{k} - \mathbf{q}))}, \end{aligned} \quad (103)$$

and the running mass $m(\Lambda)$ includes the mass counterterm and is defined by

$$\begin{aligned} m(\Lambda) &= m + M_{CT}(\Lambda) = m \left(1 - \frac{C_f g^2}{(4\pi)^2} 6 \ln \Lambda \right) \\ M_{CT}(\Lambda) &= -\delta m = -\frac{C_f g^2}{(4\pi)^2} 6m \ln \Lambda. \end{aligned} \quad (104)$$

The mass counterterm is proportional to the bare quark mass, m , and thus vanishes in the chiral limit $m \rightarrow 0$. Quark mass counterterm cancels UV divergencies. In the chiral limit, no counterterms are required. The gap equation in UV finite due to the dynamical interactions generated by flow equations.

Next we consider the quark condensate $\langle\Omega|\bar{\psi}\psi|\Omega\rangle$ for a single quark flavor. We regulate the quark condensate by subtracting the perturbative contribution

$$\begin{aligned} \langle\Omega|\bar{\psi}\psi|\Omega\rangle - \langle 0|\bar{\psi}\psi|0\rangle &= -N_c \int \frac{d\mathbf{k}}{(2\pi)^3} \left(\text{Tr} S^{(3)}(\mathbf{k}) - \text{Tr} S_0^{(3)}(\mathbf{k}) \right) \\ &= -2N_c \int \frac{d\mathbf{k}}{(2\pi)^3} \left(s(\mathbf{k}) - \frac{m}{\sqrt{k^2 + m^2}} \right), \end{aligned} \quad (105)$$

where m is the bare quark mass. As $|\mathbf{k}| \rightarrow \infty$ the mass gap $M(\mathbf{k}) \rightarrow m$ and the non-perturbative sine behaves as $s(\mathbf{k}) \rightarrow m/\sqrt{k^2 + m^2}$. Thus this subtraction improves the convergence of the quark condensate integral in the UV. Here the equal-time propagator is given by $S^{(3)}(\mathbf{k}) = 1/2\Omega [mA - \boldsymbol{\gamma} \cdot \mathbf{k}(1 + B)]$. When the scalar part of the propagator is nonzero ($mA \neq 0$), the nonzero mass gap ($M_0 = mA/(1 + B)$) and the chiral condensate ($\langle\bar{\psi}\psi\rangle_0 \sim \int dk mA/\Omega$) are generated.

We approximate the meson bound state as a valence pair of quark and antiquark, that corresponds to the Tamm-Dancoff approximation. In terms of the quasiparticle operators the TDA meson creation operator reads

$$R_n^\dagger = \int \frac{d\mathbf{q}}{(2\pi)^3} \sum_{\delta\gamma} b_\delta^\dagger(\mathbf{q}) d_\gamma^\dagger(-\mathbf{q}) \psi_n^{\delta\gamma}(\mathbf{q}), \quad (106)$$

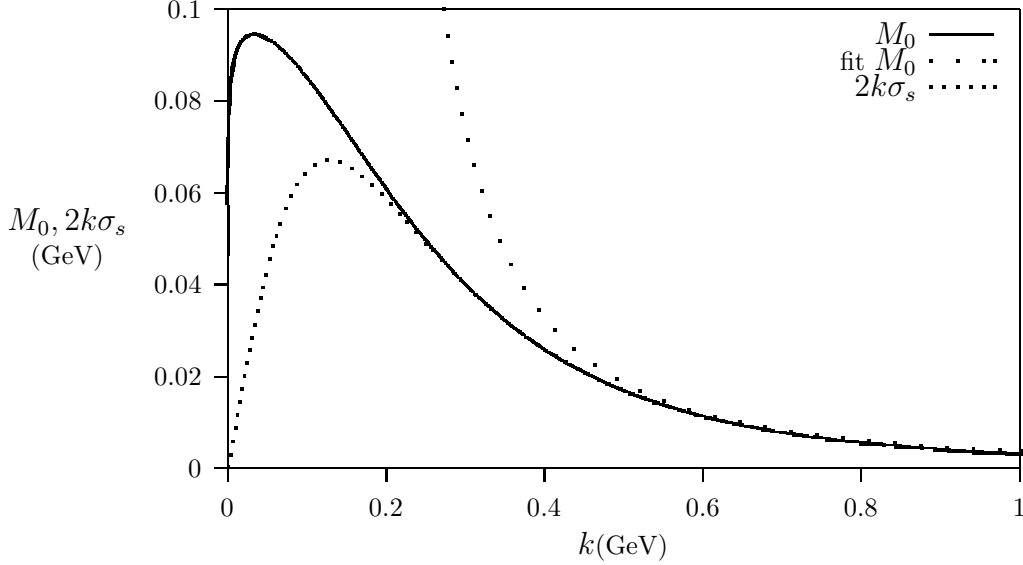


Figure 12: The numerical solution of dynamical quark mass, $M_0(k)$, and the scalar part of the propagator, $2k\sigma_s$, in the chiral limit when Coulomb and generated potentials with the running coupling $\alpha_s(k^2)$ are added to confinement. The parameters for the numerical solution of the gap equation are $\sigma = 0.18\text{GeV}^2$, $\Lambda = 1\text{GeV}$. The results are compared with the fit function given by $M_0(k) = 0.0060/(k^2[\ln(k^2/0.04)]^{0.43})$.

acting on the vacuum, it creates a meson with a wavefunction $|\psi_n\rangle$ with quantum number n ; annihilation operator defines the nonperturbative vacuum, i.e.

$$\begin{aligned} R_n^\dagger|\Omega\rangle &= |\psi_n\rangle \\ R_n|\Omega\rangle &= 0. \end{aligned} \quad (107)$$

Projecting Schrödinger equation $H_{eff}|\psi_n\rangle = E_n|\psi_n\rangle$ onto one particle-one hole truncated Fock sector, we get the TDA equation

$$\langle\Omega|[R_n, [H_{eff}, b_\alpha^\dagger(\mathbf{k})d_\beta^\dagger(-\mathbf{k})]]|\Omega\rangle = M_n\psi_n^{\alpha\beta}(\mathbf{k}), \quad (108)$$

where the binding energy is defined as $M_n = E_n - E_0$. Commutation relation of the meson operators

$$\langle\Omega|[R_{n'}, R_n^\dagger]|\Omega\rangle = N\delta_{nn'}, \quad (109)$$

leads to a normalization condition for the wave functions

$$\int \frac{d\mathbf{q}}{(2\pi)^3} \sum_{\delta\gamma} \psi_{n'}^{\delta\gamma*}(\mathbf{q})\psi_n^{\delta\gamma}(\mathbf{q}) = N\delta_{nn'}, \quad (110)$$

with the normalization constant N .

In the Random Phase Approximation, we allow in addition to the $q\bar{q}$ creation the $q\bar{q}$ annihilation in vacuum, with corresponding wave functions X and Y for each correlation.

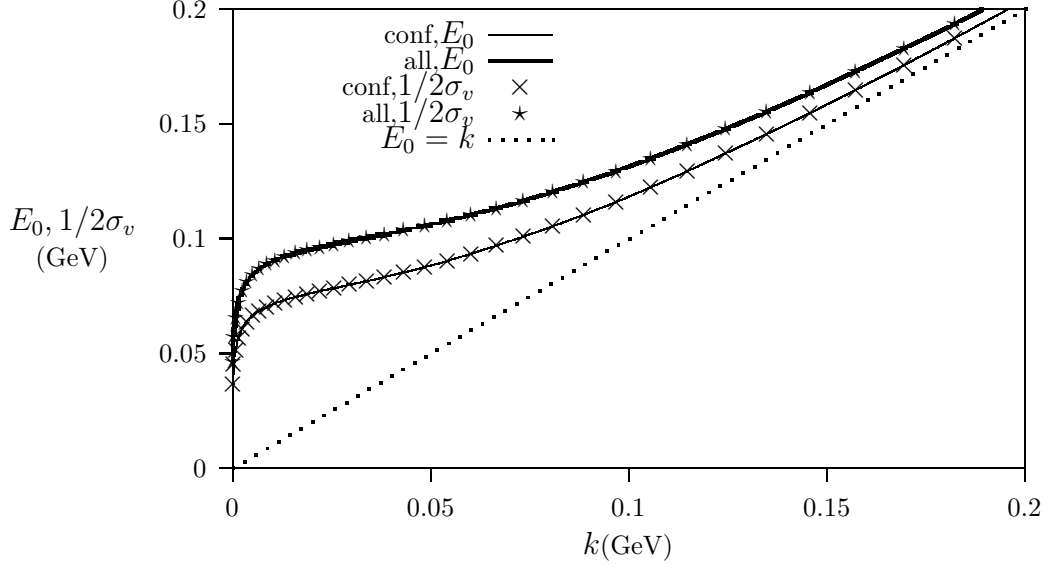


Figure 13: One particle dispersion relation, $E_0(k) = \sqrt{k^2 + M_0(k)^2}$, free dispersion, $E_0(k) = k$, and the vector part of the propagator, $1/2\sigma_v$, in the chiral limit with confinement and with confinement plus perturbative potentials (i.e. when Coulomb and generated potentials are added). The parameters are same as in Fig. 12.

Corresponding generalization of the operator given by Eq. (106) contains meson creation and annihilation terms

$$Q_n^\dagger = \int \frac{d\mathbf{q}}{(2\pi)^3} \sum_{\delta\gamma} \left[b_\delta^\dagger(\mathbf{q}) d_\gamma^\dagger(-\mathbf{q}) X_n^{\delta\gamma}(\mathbf{q}) - b_\delta(\mathbf{q}) d_\gamma(-\mathbf{q}) Y_n^{\delta\gamma}(\mathbf{q}) \right]. \quad (111)$$

The RPA wavefunction and the RPA vacuum are defined by

$$\begin{aligned} Q_n^\dagger |\Omega\rangle &= |\psi_n\rangle \\ Q_n |\Omega\rangle &= 0, \end{aligned} \quad (112)$$

where, though the same notations were used above, they should not be confused with the TDA wave function and TDA vacuum. The RPA bound state equation is given as a system of equations for both components of the wave function, X and Y ,

$$\begin{aligned} \langle \Omega | [Q_n, [H_{eff}, b_\alpha^\dagger(\mathbf{k}) d_\beta^\dagger(-\mathbf{k})]] | \Omega \rangle &= M_n X_n^{\alpha\beta}(\mathbf{k}) \\ \langle \Omega | [Q_n, [H_{eff}, b_\alpha(\mathbf{k}) d_\beta(-\mathbf{k})]] | \Omega \rangle &= M_n Y_n^{\alpha\beta}(\mathbf{k}), \end{aligned} \quad (113)$$

From the meson commutation relation

$$\langle \Omega | [Q_{n'}, Q_n^\dagger] | \Omega \rangle = N \delta_{nn'}, \quad (114)$$

the following normalization condition for the wave function components, X and Y , is obtained

$$\int \frac{d\mathbf{q}}{(2\pi)^3} \sum_{\delta\gamma} \left[X_{n'}^{\delta\gamma*}(\mathbf{q}) X_n^{\delta\gamma}(\mathbf{q}) - Y_{n'}^{\delta\gamma*}(\mathbf{q}) Y_n^{\delta\gamma}(\mathbf{q}) \right] = N \delta_{nn'}, \quad (115)$$

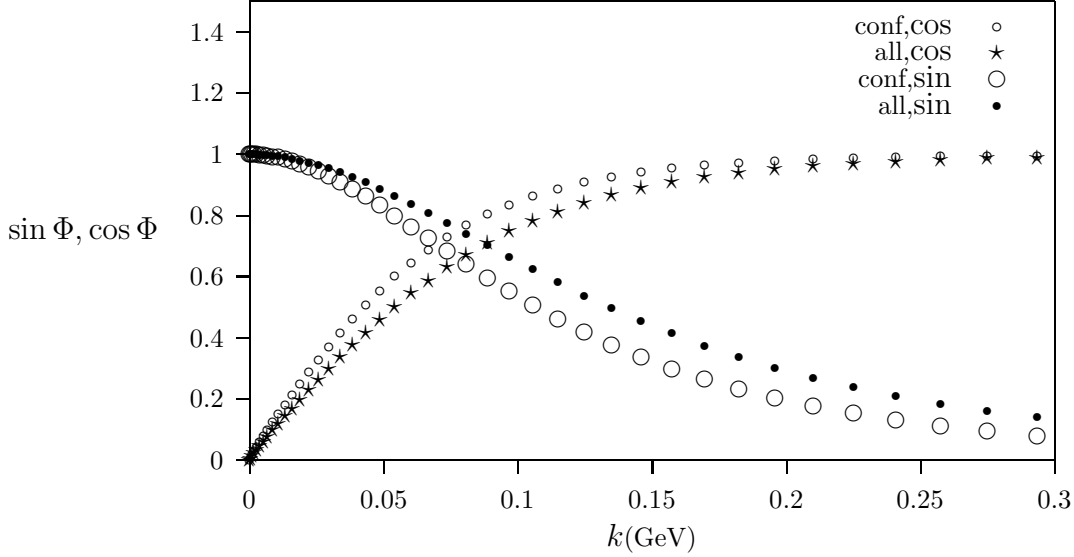


Figure 14: Sine and cosine of the Bogoliubov-Valatin angle in the chiral limit with confinement and with confinement plus perturbative potentials (i.e. when Coulomb and generated potentials are added). The parameters are same as in Fig. 12.

with the normalization constant N .

We considered pseudoscalar π -meson ($J^{PC} = 0^{++}$ $L = S = 1, J = 0$) and vector ρ -meson ($J^{PC} = 0^{-+}$ $L = S = J = 0$) channels to illustrate effects of the chiral symmetry breaking. Based on quantum numbers of these states, the tensor structure of π - and ρ -wave functions can be identified as

$$\begin{aligned} X_{\pi}^{\alpha\beta}(\mathbf{k}) &= (i\sigma_2)^{\alpha\beta} X_{\pi}(\mathbf{k}), \quad Y_{\pi}^{\alpha\beta}(\mathbf{k}) = (-i\sigma_2)^{\alpha\beta} Y_{\pi}(\mathbf{k}) \\ X_{\rho}^{\alpha\beta}(\mathbf{k}) &= (\sigma i\sigma_2)^{\alpha\beta} X_{\rho}(\mathbf{k}), \quad Y_{\rho}^{\alpha\beta}(\mathbf{k}) = (-i\sigma_2\sigma)^{\alpha\beta} Y_{\rho}(\mathbf{k}). \end{aligned} \quad (116)$$

Normalization is chosen

$$\int \frac{d\mathbf{k}}{(2\pi)^3} (X^*(\mathbf{k})X(\mathbf{k}) - Y^*(\mathbf{k})Y(\mathbf{k})) = 1, \quad (117)$$

reducing the normalization constant of the full wave function to

$$N = \langle \psi_n | \psi_n \rangle = 2N_c, \quad (118)$$

where factor 2 comes from trace in the spinor space, and $N_c = 3$. The RPA equations for the momentum wave function components $X(\mathbf{k}), Y(\mathbf{k})$ have the same form for π and ρ states

$$M_n X(\mathbf{k}) = 2\varepsilon(\mathbf{k})X(\mathbf{k}) - \int \frac{q^2 dq dx}{4\pi^2} I_{xx}(\mathbf{k}, \mathbf{q})X(\mathbf{q}) - \int \frac{q^2 dq dx}{4\pi^2} I_{xy}(\mathbf{k}, \mathbf{q})Y(\mathbf{q})$$

$$\begin{aligned}
& - \int \frac{q^2 dq dx}{4\pi^2} G_{xx}(\mathbf{k}, \mathbf{q}) X(\mathbf{q}) - \int \frac{q^2 dq dx}{4\pi^2} G_{xy}(\mathbf{k}, \mathbf{q}) Y(\mathbf{q}) \\
-M_n Y(\mathbf{k}) &= 2\varepsilon(\mathbf{k}) Y(\mathbf{k}) - \int \frac{q^2 dq dx}{4\pi^2} I_{yy}(\mathbf{k}, \mathbf{q}) Y(\mathbf{q}) - \int \frac{q^2 dq dx}{4\pi^2} I_{yx}(\mathbf{k}, \mathbf{q}) X(\mathbf{q}) \\
& - \int \frac{q^2 dq dx}{4\pi^2} G_{yy}(\mathbf{k}, \mathbf{q}) Y(\mathbf{q}) - \int \frac{q^2 dq dx}{4\pi^2} G_{yx}(\mathbf{k}, \mathbf{q}) X(\mathbf{q}), \quad (119)
\end{aligned}$$

where the kernels I and G for π are given by

$$\begin{aligned}
I_{xx}^\pi(\mathbf{k}, \mathbf{q}) &= I_{yy}^\pi(\mathbf{k}, \mathbf{q}) = C_f V_{L+C}(\mathbf{k}, \mathbf{q}) \frac{1}{2} [(1+s(\mathbf{k}))(1+s(\mathbf{q})) \\
& + (1-s(\mathbf{k}))(1-s(\mathbf{q})) + 2c(\mathbf{k})c(\mathbf{q})x] \\
I_{xy}^\pi(\mathbf{k}, \mathbf{q}) &= I_{yx}^\pi(\mathbf{k}, \mathbf{q}) = C_f V_{L+C}(\mathbf{k}, \mathbf{q}) \frac{1}{2} [-(1+s(\mathbf{k}))(1-s(\mathbf{q})) \\
& - (1-s(\mathbf{k}))(1+s(\mathbf{q})) + 2c(\mathbf{k})c(\mathbf{q})x] \\
G_{xx}^\pi(\mathbf{k}, \mathbf{q}) &= G_{yy}^\pi(\mathbf{k}, \mathbf{q}) = 2C_f W_1(\mathbf{k}, \mathbf{q}) \frac{1}{2} \left[-(1+s(\mathbf{k}))(1-s(\mathbf{q})) \right. \\
& \left. - (1-s(\mathbf{k}))(1+s(\mathbf{q})) - 2c(\mathbf{k})c(\mathbf{q}) \frac{(1+x^2)kq - x(k^2+q^2)}{(\mathbf{k}-\mathbf{q})^2} \right] \\
G_{xy}^\pi(\mathbf{k}, \mathbf{q}) &= G_{yx}^\pi(\mathbf{k}, \mathbf{q}) = 2C_f W_2(\mathbf{k}, \mathbf{q}) \frac{1}{2} \left[(1+s(\mathbf{k}))(1+s(\mathbf{q})) \right. \\
& \left. + (1-s(\mathbf{k}))(1-s(\mathbf{q})) - 2c(\mathbf{k})c(\mathbf{q}) \frac{(1+x^2)kq - x(k^2+q^2)}{(\mathbf{k}-\mathbf{q})^2} \right], \quad (120)
\end{aligned}$$

and for ρ are given by

$$\begin{aligned}
I_{xx}^\rho(\mathbf{k}, \mathbf{q}) &= I_{yy}^\rho(\mathbf{k}, \mathbf{q}) = C_f V_{L+C}(\mathbf{k}, \mathbf{q}) \frac{1}{2} \left[(1+s(\mathbf{k}))(1+s(\mathbf{q})) \right. \\
& \left. + \frac{1}{3}(1-s(\mathbf{k}))(1-s(\mathbf{q}))(4x^2-1) + 2c(\mathbf{k})c(\mathbf{q})x \right] \\
I_{xy}^\rho(\mathbf{k}, \mathbf{q}) &= I_{yx}^\rho(\mathbf{k}, \mathbf{q}) = C_f V_{L+C}(\mathbf{k}, \mathbf{q}) \frac{1}{2} \left[-\frac{1}{3}(1+s(\mathbf{k}))(1-s(\mathbf{q})) \right. \\
& \left. - \frac{1}{3}(1-s(\mathbf{k}))(1+s(\mathbf{q})) + \frac{2}{3}c(\mathbf{k})c(\mathbf{q})x \right] \\
G_{xx}^\rho(\mathbf{k}, \mathbf{q}) &= G_{yy}^\rho(\mathbf{k}, \mathbf{q}) = C_f W_1(\mathbf{k}, \mathbf{q}) \frac{1}{2} \left[\frac{1}{3}(1+s(\mathbf{k}))(1-s(\mathbf{q})) \left(1 - \frac{2(1-x^2)k^2}{(\mathbf{k}-\mathbf{q})^2} \right) \right. \\
& \left. + \frac{1}{3}(1-s(\mathbf{k}))(1+s(\mathbf{q})) \left(1 - \frac{2(1-x^2)q^2}{(\mathbf{k}-\mathbf{q})^2} \right) - \frac{2}{3}c(\mathbf{k})c(\mathbf{q}) \left(x + \frac{(1-x^2)kq}{(\mathbf{k}-\mathbf{q})^2} \right) \right] \\
G_{xy}^\rho(\mathbf{k}, \mathbf{q}) &= G_{yx}^\rho(\mathbf{k}, \mathbf{q}) = C_f W_2(\mathbf{k}, \mathbf{q}) \frac{1}{2} \left[\frac{1}{3}(1+s(\mathbf{k}))(1+s(\mathbf{q})) \right. \\
& \left. + \frac{1}{3}(1-s(\mathbf{k}))(1-s(\mathbf{q}))(2x^2-1) + \frac{2}{3}c(\mathbf{k})c(\mathbf{q}) \left(x - \frac{(1-x^2)kq}{(\mathbf{k}-\mathbf{q})^2} \right) \right], \quad (121)
\end{aligned}$$

where $x = \hat{\mathbf{k}} \cdot \hat{\mathbf{q}}$; and we have used

$$1 - (\hat{\mathbf{k}} \cdot \hat{\mathbf{l}})^2 = \frac{(1-x^2)q^2}{(\mathbf{k}-\mathbf{q})^2}, \quad 1 - (\hat{\mathbf{q}} \cdot \hat{\mathbf{l}})^2 = \frac{(1-x^2)k^2}{(\mathbf{k}-\mathbf{q})^2}$$

	TDA, (MeV)			RPA, (MeV)		
conf.	504	1364	2115	222	1416	2298
conf.+Coul.	608	1514	2249	427	1521	2309
conf.+Coul.+gen.	513	1411	2161	180	1413	2218

Table 8: Pion spectrum for the ground, first and second excited states in the TDA and RPA approaches with confining, confining+Coulomb and confining+Coulomb+generated potentials taken. Chiral limit $m = 0$ ($\alpha_s = 0.4, \sigma = 0.18 GeV^2, \Lambda = 10 GeV$).

$$\hat{\mathbf{k}} \cdot \hat{\mathbf{l}} \hat{\mathbf{q}} \cdot \hat{\mathbf{l}} = \frac{x(k^2 + q^2) - (1 + x^2)kq}{(\mathbf{k} - \mathbf{q})^2}, \quad (122)$$

with $\mathbf{l} = \mathbf{k} - \mathbf{q}$.

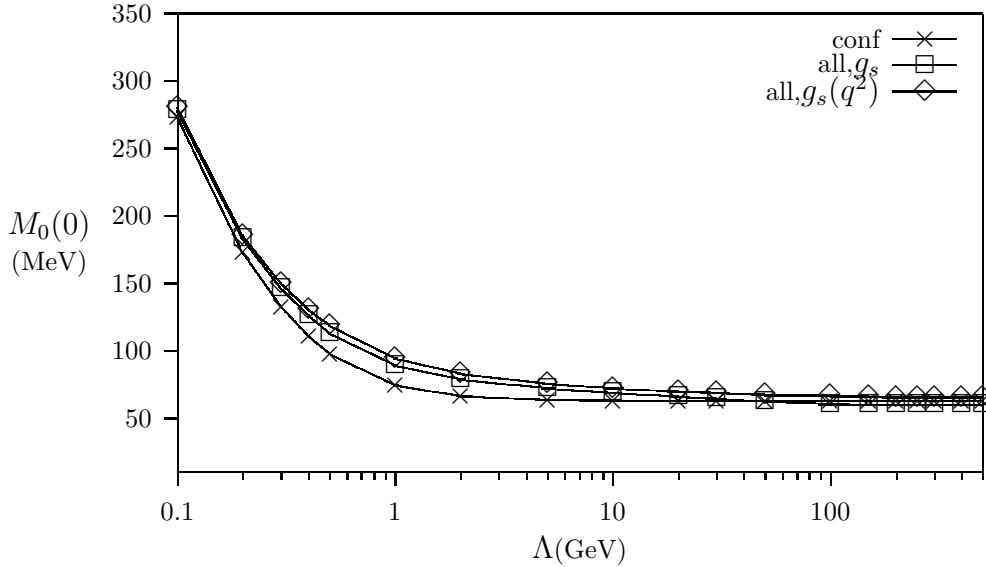


Figure 15: Cut-off dependence of the constituent quark mass in the chiral limit (same parameters as in Fig. 12). Crosses represent solution with confinement. Boxes [diamonds] represent solution when Coulomb and generated potentials are added with the constant value of coupling g_s [with the running coupling $g_s(q^2)$].

Numerical results

For the numerical calculations we have used the routines from the SLATEC linear algebra archive, part of the Netlib database maintained by UTK and ORNL. The routines are found at www.netlib.org/slatec/lin/ and a description of the entire SLATEC archive can be found at www.netlib.org/slatec/toc.

Effective quark mass and energy are shown in Figures 12 and 13, respectively. At large momenta effective mass vanishes and the energy tends to the perturbative value, $E(\mathbf{k}) = k$, while for zero momentum, the energy tends to the constant, which we refer as

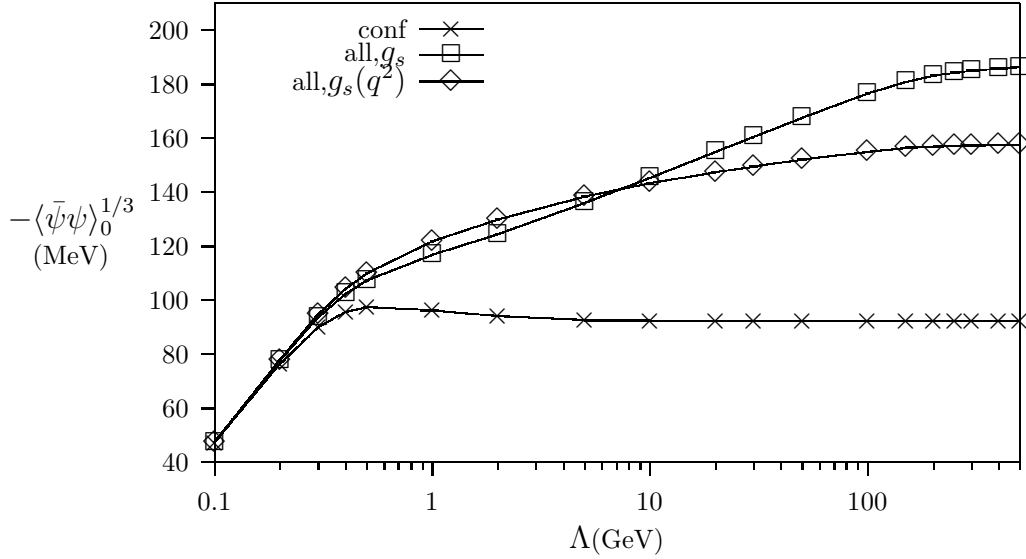


Figure 16: Quark condensate cut-off dependence in the chiral limit (same parameters as in Fig. 12). Crosses represent solution with confinement. Boxes [diamonds] represent solution when Coulomb and generated potentials are added with the constant value of coupling g_s [with the running coupling $g_s(q^2)$].

m, (MeV)	TDA, (MeV)			RPA, (MeV)		
150	1038	1926	2936	1037	1986	3077
100	885	1762	2697	868	1811	2826
50	716	1590	2431	660	1626	2537
10	553	1446	2212	366	1460	2283
5	532	1428	2186	293	1437	2250
0	513	1411	2161	180	1413	2218

Table 9: Pion spectrum for the ground, first and second excited states in the TDA and RPA approaches for different current masses of constituents. Confining+Coulomb+generated potentials are taken, the same parameters as in the Table 8.

the constituent quark mass. No counterterms are required in the chiral limit. Due to the dynamical interactions we recover the large momentum behavior correctly, corresponding to the UV asymptotic region, which behavior is obtained in the course of explicit numerical solutions of the QCD renormalization group and operator product expansion and QCD sum rules.

At low momenta cosine behaves linearly (Fig. 14), with the slope $1/M(0)$ (inverse of quark constituent mass), $c(\mathbf{k}) = \mathbf{k}/M(0)$.

The sensitivity of the constituent quark mass, $M(0)$, and the chiral condensate in the chiral limit to the cut-off Λ is displayed in Figures 15 and 16. Only when all terms,

	TDA, (MeV)			RPA, (MeV)		
conf.	659	1484	2258	642	1482	2256
conf.+Coul.	750	1678	2515	732	1676	2514
conf.+Coul.+gen.	718	1592	2377	700	1590	2376

Table 10: Spectrum of the ρ meson for the ground, first and second excited states in the TDA and RPA approaches with confining, confining+Coulomb and confining+Coulomb+generated potentials taken. Chiral limit $m = 0$, the same parameters as in the Table 8.

m, (MeV)	TDA, (MeV)			RPA, (MeV)		
150	1130	2086	3247	1128	2086	3247
100	986	1916	2990	983	1915	2990
50	839	1744	2692	833	1744	2692
10	727	1616	2436	714	1615	2435
5	719	1603	2406	704	1601	2405
0	718	1592	2377	700	1590	2376

Table 11: Spectrum of the ρ meson for the ground, first and second excited states in the TDA and RPA approaches for different current masses of constituents. Confining+Coulomb+generated potentials are taken, the same parameters as in the Table 8.

instantaneous and dynamical interactions are added, we obtain the stable result. This proves that the gap equation is renormalized completely. We need to add the renormalization group running of the coupling to renormalize the condensate. For the first time, completely renormalized stable mass and condensate are obtained in the chiral limit, with values $M_0(0) = 70 \text{ MeV}$ and $\langle \bar{\psi}\psi \rangle_0 = -(155 \text{ MeV})^3$. Flow equations improve the chiral condensate by 68%.

Relative scales of constituent masses are obtained: for the gluon $< 1 \text{ GeV}$, for the s -quark $> 200 \text{ MeV}$, for the u, d -quarks $< 100 \text{ MeV}$.

Results for the pion and ρ -meson masses in RPA and TDA approaches are presented in Tables 8-11. In the chiral limit RPA gives ground state pion masses which are significantly lower than those obtained using TDA. Including the dynamical interaction terms reduces ground state pion mass even more, increasing the mass splitting between the pion and ρ meson (Tables 8 and 10). In the chiral limit we get

$$\begin{aligned}
M_\pi &= 180 \text{ MeV}, \quad M_\rho = 700 \text{ MeV} \\
M_\rho - M_\pi &= 520 \text{ MeV}.
\end{aligned}
\tag{123}$$

The $\pi - \rho$ mass splitting of 520 MeV in the chiral limit is close enough to the lattice data splitting of 600 MeV . However, we are unable to get zero mass pion either in the BCS or adding the leading order flow equations corrections. One of the reasons is break of the covariance in this model. Flow equations improve the $\pi - \rho$ mass splitting by 32% in the TDA and by 24% in the RPA.

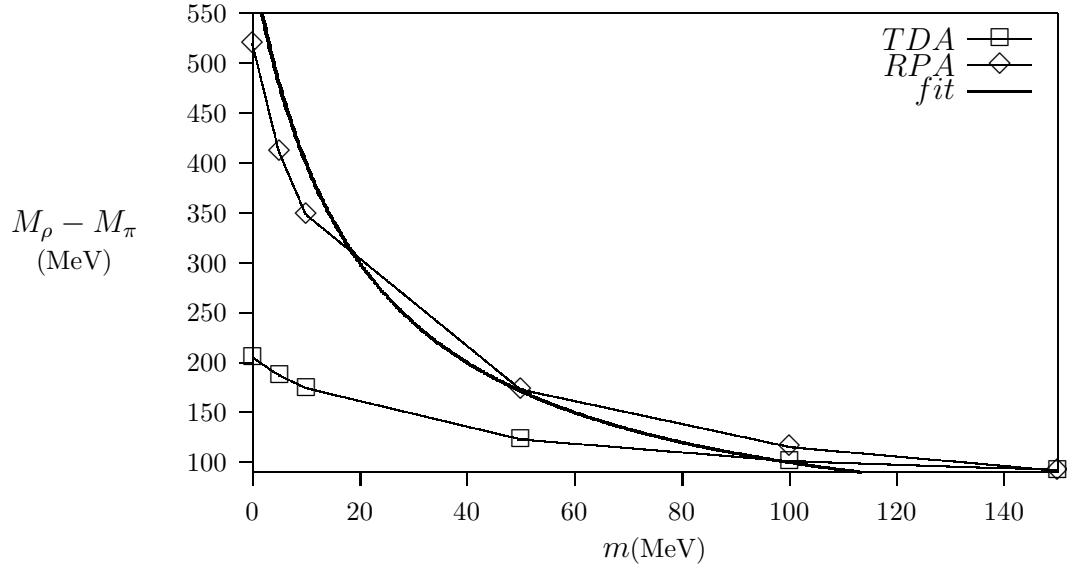


Figure 17: $\pi - \rho$ mass splitting for the ground state in TDA and RPA approaches. Chiral limit, $m = 0$, and confining+Coulomb+generated interactions are taken (same parameters as in the Table 8). Fit function is $12000/(m+20)$.

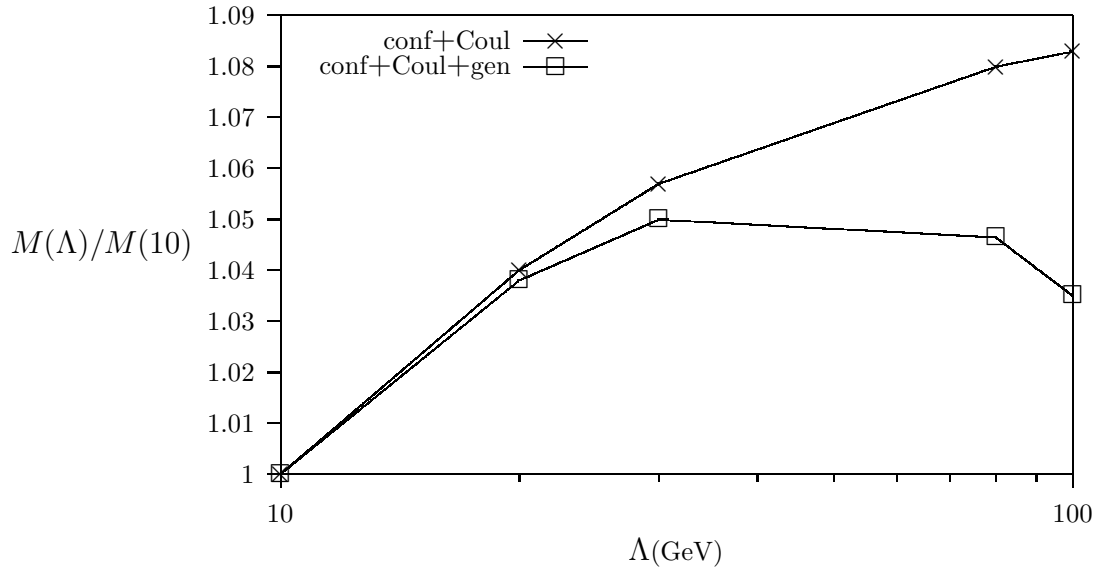


Figure 18: Cut-off dependence of the pion mass in the chiral limit $M(\Lambda)$, normalized to the pion mass at $\Lambda = 10\text{GeV}$, $M(10)$, (same parameters as in the Table 8). Line with crosses represents RPA solution with confinement+Coulomb, the line with boxes stays for RPA solution when generated potentials are added.

Numerically obtained dependence of the $\pi-\rho$ mass splitting, $M_\rho - M_\pi$, as a function of the bare mass of one of the quarks is shown in Figure 17. We find $1/m_{const}$ behavior, where m_{const} is a constituent quark mass, which is valid for heavy quarks and continues to be valid for lighter constituent quarks. This fall of is more rapid in the RPA than in the TDA approach. From the RPA fit function, a constituent quark mass can be approximated, uniformly for heavy and light quarks, as $m_{const} = m + 20 (MeV)$, with the bare quark mass m . The $1/m_{const}$ behavior is characteristic for the hyperfine interaction. We find in the chiral limit, that in the TDA roughly 30% of the $\pi-\rho$ mass splitting is due to the presence of the hyperfine interaction and 70% due to the chiral symmetry breaking. In the RPA this ratio is 40% for the hyperfine and 60% for the chiral symmetry breaking. However, the numerical value of this ratio depends on the details of the confining interaction.

The dependence of the pion mass in the chiral limit on the cut-off parameter, $M(\Lambda)$, is shown in Fig. 18. The RPA solution, with only confining+Coulomb potential included, grows unlimited (due to Coulomb), while adding the generated term stabilizes $M(\Lambda)$, which saturates roughly at $M(10)$. Stable result confirms that the TDA/RPA equations are completely renormalized when the generated by flow equations terms are included.

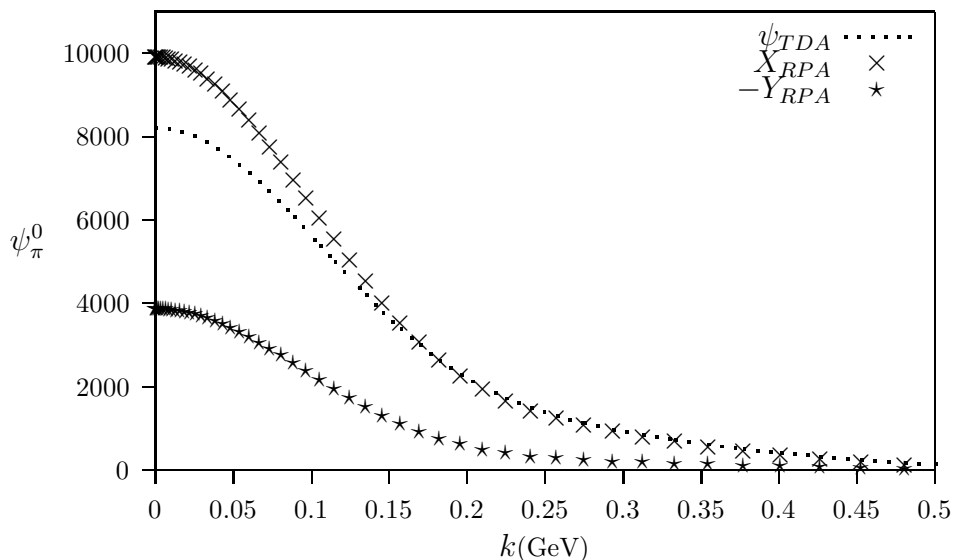


Figure 19: Ground state pion wave function in TDA and RPA approaches. Chiral limit, $m = 0$, and confining+Coulomb+generated interactions are taken ($\alpha_s = 0.4, \sigma = 0.18 GeV^2, \Lambda = 10 GeV$).

Pion wave functions for the ground and first excited states are depicted at Figures 19 and 20. Using the TDA and RPA wave functions, we obtained the pion decay constants. Though we obtained low value of quark condensate $-(155 MeV)^3$, we obtain a realistic pion decay constant, $92 MeV$, in the RPA.

Summary III

1) For the first time, due to the dynamical interactions, the UV and IR finite equations

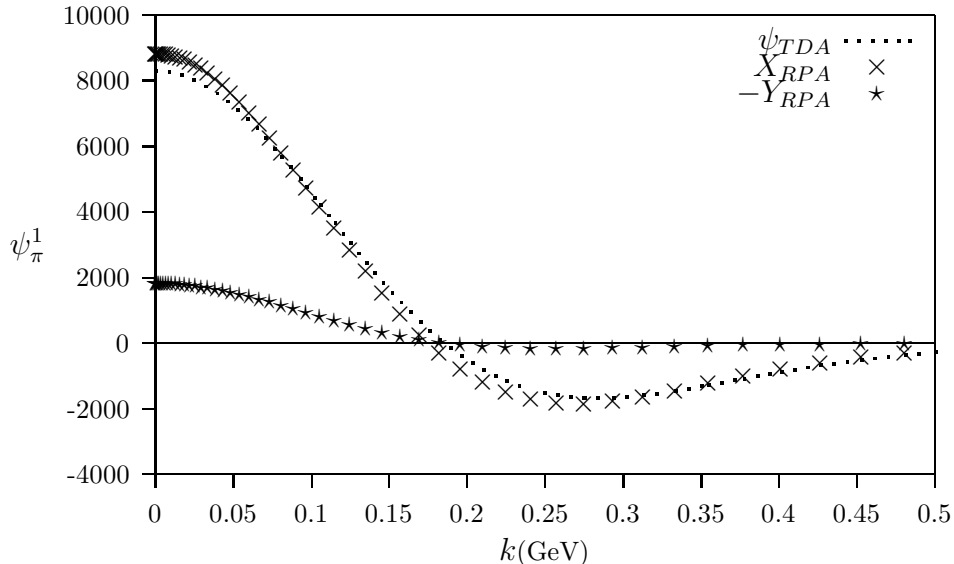


Figure 20: Pion wave function for the first excited state in TDA and RPA approaches. Chiral limit, $m = 0$, and confining+Coulomb+generated interactions are taken into account (same parameters as in Fig. 17).

are obtained in many-body technique. In the chiral limit, no additional UV renormalization is required (no momentum dependent counterterms).

2) For the first time, the instantaneous as well as dynamical interactions are included (In this way we have utilized the success of the BCS model, where nonperturbative features such as dynamical chiral symmetry breaking and massive quasiparticle modes are explicitly present, and included perturbatively dynamical interactions in the BCS framework). In the RPA roughly 40% of the $\pi - \rho$ mass splitting is due to the presence of the hyperfine interaction and 60% due to the chiral symmetry breaking (link between different model calculations).

3) Due to the dynamical interactions, closed Ward-Takashi identities are obtained. Though we work in the gauge theory, there are no ambiguities, since all fields in the effective Hamiltonian are physical.

3 Conclusions

In this work we have outlined a strategy to derive an effective renormalized Hamiltonian by means of flow equations. Application of the flow equations with the condition, that particle number conserving terms are considered diagonal and those changing the particle number off-diagonal led as in other cases to useful effective Hamiltonians.

The main advantage of flow equations as compared to other many-body approaches is, that states of different particle number are completely decoupled, since the particle number violating contributions are eliminated down to $\lambda = 0$. Thus one is able to truncate

the Fock space and the bound state problem reduces to an eigenstate equation in the lowest Fock sector of quasiparticles. Positronium (meson) problem is approximated as a state of two valence electrons (constituent quark and antiquark), described by a Bethe-Salpeter equation with an effective Hamiltonian in two-body sector. Energy/mass of a quasiparticle is found from the gap equation with an effective Hamiltonian in one-body sector. Coupled gap equation and Bethe-Salpeter equation with effective sector Hamiltonians are analyzed further analytically and numerically for a one-particle mass gap and bound state spectrum, respectively.

We applied flow equations to the light-front Hamiltonians of QED and QCD and to the Hamiltonians of gluodynamics and QCD (with dynamical quarks added) in the Coulomb gauge. We found that dynamical new terms generated by flow equations are crucial in order to obtain an agreement with covariant calculations and the experimental results. In the light-front positronium problem, due to dynamical terms triplet states are degenerate and thus rotational invariance (that means covariance in this case) is maintained. Using flow equations, we obtain the singlet-triplet splitting in the light-front framework which agrees with the experimental data.

In the Coulomb gauge QCD, due to the dynamical interactions we obtain for the first time the gap equation and the Bethe-Salpeter equation which are finite both in the UV and IR regions. We find that no additional renormalization is required in the chiral limit. For the first time, we include dynamical interactions in the framework of many-body technique where confinement and chiral symmetry breaking explicitly present. In this way we have studied an overlap of hadron physics and high energy QCD. We took into account the hyperfine interaction as well as chiral symmetry breaking and obtained the $\pi - \rho$ mass splitting caused by the instantaneous and dynamical interactions. We find in the RPA, that roughly 40% of the $\pi - \rho$ mass splitting is due to the presence of the hyperfine interaction and 60% due to the chiral symmetry breaking. Flow equations improve the gluon and quark condensates as compared with other Hamiltonian methods (we obtain $\langle \alpha/\pi F_{\mu\nu} F_{\mu\nu} \rangle = 1.3 \cdot 10^{-2} GeV^4$ agrees with the sum rules and $\langle \bar{\psi}\psi \rangle = -(155 MeV)^3$ is still low).

We find that for glueball states confinement plays the dominant role and dynamical terms are necessary to insure the correct (finite) UV behavior. However, in meson systems, dynamical terms are equally important with the instantaneous terms responsible for chiral symmetry breaking. Using flow equations, we obtain masses of low lying glueballs and mesons which agree with lattice data and the experimental results.

The main publications on this topic are:

References

- [1] E. Gubankova, F. Wegner, Phys. Rev. D**58**, 025012 (1998); E. Gubankova, H.-C. Pauli, F. Wegner, G. Papp, 'Light-cone Hamiltonian flow for positronium', hep-th/9809143.
- [2] E. Gubankova, C.-R. Ji, and S. R. Cotanch, Phys. Rev. D**62** 125012 (2000).
- [3] E. Gubankova, C.-R. Ji, and S. R. Cotanch, Phys. Rev. D**62**, 074001 (2000).
- [4] E. Gubankova, '*Flow equations for chiral problem in QCD*', hep-ph/0112213.